Title

A genome-wide CRISPR screen identifies BRD4 as a regulator of cardiomyocyte differentiation.

Journal

Nature Cardiovascular Research, 3(3)

Authors

Padmanabhan, Arun
de Soysa, T
Pelonero, Angelo
et al.

Publication Date

2024-03-01

DOI

10.1038/s44161-024-00431-1

Peer reviewed

HHS Public Access

Author manuscript

Nat Cardiovasc Res. Author manuscript; available in PMC 2024 August 29.

Published in final edited form as:

Nat Cardiovasc Res. 2024 March ; 3(3): 317–331. doi:10.1038/s44161-024-00431-1.

A Genome-Wide CRISPR Screen Identifies BRD4 as a Regulator of Cardiomyocyte Differentiation

Arun Padmanabhan[1,2,3,†], **Yvanka de Soysa**[1], **Angelo Pelonero**[1], **Valerie Sapp**[4,5], **Parisha P. Shah**[6,7], **Qiaohong Wang**[6,7], **Li Li**[6,7], **Clara Youngna Lee**[1,2], **Nandhini Sadagopan**[1,2], **Tomohiro Nishino**[1], **Lin Ye**[1], **Rachel Yang**[6,7], **Ashley Karnay**[6,7], **Andrey Poleshko**[7], **Nikhita Bolar**[6,7], **Ricardo Linares-Saldana**[6,7], **Sanjeev S. Ranade**[1], **Michael Alexanian**[1], **Sarah U. Morton**[8,9], **Mohit Jain**[4,5], **Saptarsi M. Haldar**[1,2,13], **Deepak Srivastava**[1,10,11,12,†], **Rajan Jain**[6,7,†]

[1]Gladstone Institutes; San Francisco, CA, USA

[2]Department of Medicine, University of California, San Francisco School of Medicine; San Francisco, CA, USA

[3]Chan Zuckerberg Biohub San Francisco; San Francisco, CA, USA

[4]Department of Medicine, University of California, San Diego School of Medicine; San Diego, CA, USA

[5]Department of Pharmacology, University of California, San Diego; San Diego, CA, USA

[6]Cardiovascular Institute, Epigenetics Institute, and Department of Medicine, Perelman School of Medicine, University of Pennsylvania; Philadelphia, PA, USA

[7]Department of Cell and Developmental Biology, University of Pennsylvania; Philadelphia, PA, USA

[8]Division of Newborn Medicine, Boston Children's Hospital; Boston, MA, USA

[9]Department of Pediatrics, Harvard Medical School; Boston, MA, USA

[10]Department of Pediatrics, University of California, San Francisco School of Medicine; San Francisco, CA, USA

[11]Roddenberry Center for Stem Cell Biology and Medicine at Gladstone Institutes; San Francisco, CA, USA

[12]Department of Biochemistry and Biophysics, University of California, San Francisco; San Francisco, CA, USA

[†] arun.padmanabhan@gladstone.ucsf.edu, deepak.srivastava@gladstone.ucsf.edu, jainr@pennmedicine.upenn.edu.

Author Contributions

A.P., R.J. and D.S. conceived and designed the study. A.P., Y.d.S., V.S., P.P.S., Q.W., L.L., C.Y.L., N.S., A. Poleshko, N.B., R.L.-S., T.N. and L.Y. performed all the experiments. A.P., Y.d.S., V.S., A. Pelonero, S.U.M., M.J., R.Y., A.K., L.Y. and R.J. analyzed the data. M.A., S.M.H. and D.S. assisted with data interpretation. A.P. and R.J. wrote the manuscript. D.S. and R.J. supervised the project. All authors edited and approved the manuscript.

Competing Interests

D.S. is a scientific co-founder, shareholder and director of Tenaya Therapeutics. S.M.H. is an executive, officer and shareholder of Amgen and is a scientific co-founder and shareholder of Tenaya Therapeutics. M.J. is founder, shareholder and executive of Sapient Bioanalytics, LLC. The remaining authors declare no competing interests.

[13]Present address: Amgen Research, Cardiometabolic Disorders; South San Francisco, CA, USA

Abstract

Human induced pluripotent stem cell (hiPSC) to cardiomyocyte (CM) differentiation has reshaped approaches to studying cardiac development and disease. In this study, we employed a genome-wide CRISPR screen in a hiPSC to CM differentiation system and reveal here that BRD4, a member of the bromodomain and extraterminal (BET) family, regulates CM differentiation. Chemical inhibition of BET proteins in mouse embryonic stem cell (mESC)- derived or hiPSC-derived cardiac progenitor cells (CPCs) results in decreased CM differentiation and persistence of cells expressing progenitor markers. *In vivo*, BRD4 deletion in second heart field (SHF) CPCs results in embryonic or early postnatal lethality, with mutants demonstrating myocardial hypoplasia and an increase in CPCs. Single-cell transcriptomics identified a subpopulation of SHF CPCs that is sensitive to BRD4 loss and associated with attenuated CM lineage-specific gene programs. These results highlight a previously unrecognized role for BRD4 in CM fate determination during development and a heterogenous requirement for BRD4 among SHF CPCs.

Introduction

Congenital heart diseases (CHDs) remain a leading cause of childhood morbidity and mortality and represent the most common birth defect[1]. In approximately 40% of CHD cases, genetic or environmental causes can be identified, with only a small fraction attributable to single-gene disorders and the remainder accounted for by gross chromosomal anomalies, pathogenic copy number variants or syndromic presentations[2]. The large unexplained portion of CHD is thought to be multifactorial, resulting from oligogenic patterns of inheritance or combinations of genetic and environmental factors[3]. Studying the molecular underpinnings of cardiac development is essential for understanding of CHD pathogenesis.

Techniques to differentiate human induced pluripotent stem cells (hiPSCs) into specific cardiac lineages *in vitro*, including cardiomyocytes (CMs), have advanced the ability to interrogate molecular mechanisms underlying cardiac homeostasis and disease. During cardiogenesis, cardiac progenitor cells (CPCs) give rise to the various cell types of the mature heart, including CMs, endothelial cells and smooth muscle cells. CMs arise primarily from two progenitor cell pools, termed the first and second heart fields (FHFs and SHFs). Understanding of the contribution of these heart fields to cardiogenesis *in vivo* has been aided by Cre recombinase alleles driven by regulatory elements that specifically mark these individual pools. Such approaches, when coupled with manipulation of specific genes and unbiased interrogation of cell state, have provided key insights into the mechanisms of cardiac development and CHD pathogenesis[4].

In the present study, we performed a genome-wide CRISPR-based genetic loss-of-function screen in hiPSCs to identify novel regulators of CM lineage commitment and differentiation. We discovered that the transcriptional co-activator BRD4, a member of the bromodomain and extraterminal (BET) family of proteins, regulates CPC differentiation. Using a combination of *in vitro* differentiation approaches and conditional mouse models, we show

that BRD4 orchestrates CPC gene programs and identify a specific population of CPCs that is sensitive to BRD4 loss. As variants in *BRD4* have been described in patients with CHD[5,6], our findings demonstrate the importance of BRD4 in cardiogenesis and provide mechanistic insight into BRD4 function in the developing heart.

Results

CRISPR screening identifies regulators of CM differentiation

To identify genes relevant to CM differentiation *in vitro* that may lead to novel insights into cardiac development *in vivo*, we performed a genome-wide CRISPR knockout screen in a hiPSC to CM differentiation system (Fig. 1a). The human CRISPR 'Brunello' lentiviral pooled library[7], consisting of 76,441 single guide RNAs (sgRNAs), was introduced into undifferentiated hiPSCs (IPSL1) such that approximately 92% of the CRISPR-Cas9 library sgRNAs were present in hiPSCs at 10 read counts or higher[8]. hiPSCs underwent antibiotic selection to enrich for sgRNA transduction and were reserved for the undifferentiated control condition or differentiated to CMs. We identified sgRNAs that were overrepresented (enriches hiPSC:CM differentiation) or underrepresented (depletes hiPSC:CM differentiation) when compared to those in the undifferentiated control condition (Fig. 1a, Extended Data Fig. 1a and Supplementary Dataset 1). Broadly categorizing the top 200 hits by biological process (Extended Data Fig. 1b–e) revealed heterologous terms. We identified 306 genes in our enrichment analysis and 898 in our depletion analysis, representing loci that promote or repress hiPSC:CM differentiation, respectively (Benjamini-Hochberg- corrected $P < 0.02$ with 5% false discovery rate (FDR)). The larger depletion cohort is expected given that loss of genes important for hiPSC survival and mesoderm commitment would be in this category. Our screen identified *CAV1* and *ZIC2* as promoting[9,10] and *CBY1* and *ACVR1* as inhibiting CM differentiation[11,12], consistent with previous reports.

We next sought to determine if those genes whose loss of function affected CM differentiation in our screen may be enriched for damaging mutations in humans with CHD. Efforts seeking to better understand the genetic underpinnings of CHD have prompted phenotyping of cohorts of affected patients coupled with genomic sequencing[5,13]. We assessed the frequency of *de novo* loss of function or damaging missense variants (as defined by the MetaSVM algorithm[14]) in the 1,204 hits from our screen among 3,526 patients with CHD enrolled in the Pediatric Cardiac Genomic Consortium, the largest available cohort of parent-offspring trios with CHD who have undergone whole-exome sequencing[2], and compared this to 1,789 non-CHD participants[15]. We found an increased burden of damaging *de novo* variants (DNVs) in patients with CHD (99 in CHD cohort versus 23 in non-CHD cohort, $P = 3.6 \times 10^{-4}$; Extended Data Fig. 1f,g and Supplementary Dataset 2). Upon eliminating patients with CHD with loss of function variants in one of 78 known dominant CHD genes[2], the increased burden of damaging DNVs in the 1,204 hits from our screen persisted (86 in CHD cohort versus 23 in non-CHD cohort, $P = 1.8 \times 10^{-3}$; Extended Data Fig. 1f,g and Supplementary Dataset 2). Thus, the top hits from our CRISPR-based screen identified genes enriched for damaging DNVs among those with CHD.

A diverse group of targets was identified in both our enrichment and depletion analyses (Extended Data Fig. 1b–e and Supplementary Dataset 1). Among the top hits that enhance CM differentiation were *TAF5L* and *TAF6L*, two members of the p300/CBP-associated factor (PCAF) complex, a transcriptional co-activator with intrinsic histone acetylase activity[16]. *TADA1*, *TADA2B* and *SUPT20H*, three other high-ranking hits from the enrichment analysis, belong to the same protein-protein interaction network[17], with two of these proteins belonging to the Spt/Ada/Gcn5 acetyltransferase (SAGA) complex. High-ranking hits from our depletion analysis included factors involved in the ubiquitin-proteasome pathway (*UBE2H*, *HUWE1*, *PSMC1* and *SUMO4*) and in mRNA processing (*EDC4* and *SUGP2*).

Gene Ontology (GO) enrichment analysis of the statistically significant screen hits (Extended Data Fig. 1d,e) identified chromatin remodeling among the biological processes in our depletion analysis ($P = 2.12 \times 10^{-3}$) and peptide-lysine-N-acetyltransferase activity and histone acetyltransferase activity in the enrichment analyses. As chromatin remodeling complexes and histone modifications have critical roles in heart development[18], we further narrowed our hits by collecting and ranking chromatin-associated proteins represented in our screen (Fig. 1b,c). We found *BRD4*, but not *BRD2/3* or other known transcriptional co-activators (such as *EP300* and *MED1*; Supplementary Dataset 1), among the highly ranked genes in our depletion analysis. BRD4, which ranked in the top 0.7% of genes represented in our screen, belongs to the BET family of proteins along with the ubiquitously expressed BRD2/3 and the testis-specific BRDT[19]. BET proteins are characterized by tandem bromodomains (BDs) in their N-terminus that mediate acetyl-lysine binding on histones and other proteins[19], and BRD4 is loaded at lineage-specific distal regulatory elements enriched for histone acetylation[20]. The biological functions of BRD4 and other BET proteins have largely been surmised from transient knockdown studies and small-molecule compounds with shape complementarity to the acetyl-lysine binding pocket of this family. The prototypical compound in this class is JQ1, which has specificity and nanomolar affinity for the BET BDs, thereby competitively displacing them from their endogenous acetylated interaction partners in a dose-titratable manner[21]. Given the important role of BRD4 as a transcriptional co-activator, coupled with the ability to pharmacologically inhibit this protein, we focused our subsequent efforts on dissecting the role of BRD4 in cardiogenesis.

Our screen did not discriminate between individual stages during CM differentiation *in vitro*. Because BRD4 is an important mediator of lineage-specific gene expression in adipocyte differentiation from pre-adipocyte progenitors[22], we hypothesized that it may be involved in differentiation of CPCs into CMs. We began by using a small-molecule approach to decipher the potential role of BRD4 in this process. We differentiated hiPSCs (WTC11) into CMs and treated them with JQ1 (ref. [21]) at day 6, corresponding to CPC specification, which resulted in reduced $TNNT2^{+}$ cell numbers by fluorescence-activated cell sorting (FACS; Extended Data Fig. 1i) at day 10. Differentiation of CPCs derived from a different hiPSC cell line (SV20) in the presence of JQ1 or MZ3 (a proteolysis-targeting chimera (PROTAC) molecule that targets BET protein degradation[23]) at day 6 resulted in reduced expression of CM genes (Fig. 1d and Extended Data Fig. 1j) at day 12. JQ1 treatment at the corresponding day of CPC specification in mESC to CM differentiation (day 5) also resulted in reduced

expression of CM genes, fewer TNNT2^{+} cells identified by FACS and reduced TNNT2 immunofluorescent staining when compared to vehicle (VEH) controls (Extended Data Fig. 2a–d). These data are consistent with our screen results and suggest that BRD4 promotes CM differentiation of CPCs.

Although our screen implicates BRD4 as a regulator of CM differentiation, a limitation of using BET inhibitors is that they target all BET family members (BRD2, BRD3 and BRD4) expressed in hiPSCs. To validate a gene-specific role for *Brd4* in CM differentiation, we derived mESCs from *CMV-CreERT2*;*Brd4*$^{flox/flox}$ blastocysts and confirmed efficient BRD4 protein depletion upon 4-hydroxytamoxifen (TAM) treatment (Extended Data Fig. 2e,f). We observed a reduction in the number of TNNT2^{+} cells at day 10 after TAM treatment at day 5 of mESC to CM differentiation, similar to treatment with JQ1 or MZ3 (Extended Data Fig. 2b). We assessed the consequences of BRD4 loss at the cardiac progenitor stage of mESC to CM differentiation on gene expression by treatment with TAM or VEH at day 5, followed by RNA sequencing (RNA-seq) at day 10 (n ≥ 3 biological replicates). We identified 1,311 differentially expressed genes, including several cardiac transcription factors and structural genes (1,056 downregulated and 255 upregulated, log 2 fold change (FC) ≥ |1|, adjusted $P < 0.05$; Extended Data Fig. 2g,h and Supplementary Table 1). GO analysis revealed enrichment for biological process terms related to CM function (for example, muscle contraction and actin-myosin filament sliding) among genes downregulated after BRD4 loss, and analysis of upregulated genes revealed enrichment for terms related to cellular stress responses (Extended Data Fig. 2g). Collectively, these studies support a critical role for BRD4 in regulating CM differentiation *in vitro* in both murine and human cellular systems.

BRD4 is necessary in SHF cells for CM differentiation

To test the necessity of BRD4 in cardiac progenitor differentiation *in vivo*, we sought to delete *Brd4* expression in murine CPCs using mouse models that drive the expression of Cre recombinase specifically in these populations. We focused on SHF CPCs given that these cells give rise to multiple cardiac cell types, and SHF differentiation occurs slightly later than FHF differentiation. We deleted BRD4 in SHF precursors expressing *Islet1* (*Isl1*) using the *Isl1-Cre* (*Isl1*$^{Cre/+}$)[24] allele and a *Brd4* conditional allele (*Brd4*^{flox}) wherein the ATG-containing third exon of *Brd4* is flanked by loxP sites[25,26]. We found no *Isl1*$^{Cre/+}$;*Brd4*$^{flox/flox}$ mutant embryos at postnatal day (P) 0 (n = 58 pups; zero observed versus 14.5 expected; $\chi^2 = 22.97$, $P < 0.005$), indicating that BRD4 loss in ISL1-expressing progenitors and their derivatives results in embryonic lethality.

We isolated mutant (*Isl1*$^{Cre/+}$;*Brd4*$^{flox/flox}$) and control (*Brd4*$^{flox/flox}$ or *Isl1*$^{Cre/+}$;*Brd4*$^{flox/+}$) embryos at multiple embryonic timepoints and confirmed efficient deletion of BRD4 (Fig. 2 and Extended Data Fig. 3). At mid-gestation, *Isl1*$^{Cre/+}$;*Brd4*$^{flox/flox}$ mutants demonstrated significantly reduced right ventricle (RV) thickness when compared to littermate controls (embryonic day (E) 12.5, 44.7 μm versus 20.6 μm, n = 2, $P < 0.0001$; E14, 91.6 μm versus 31.6 μm, n ≥ 2, $P = 0.0091$; Fig. 2a–h and Extended Data Fig. 3a,b). Immunohistochemical assessment of proliferation and apoptosis in the RV and outflow tract

(OFT) at similar timepoints demonstrated no statistically significant differences between mutants and littermate controls (Extended Data Fig. 3c).

Mutant embryos demonstrated subtle thinning of the RV and OFT when compared to littermate controls earlier in gestation (~E9.5–10), where we and others have shown that $ISL1^+$ progenitors populate the distal OFT and differentiate into CMs[27] (8.2 μm versus 6.5 μm, n = 3, $P = 0.0021$; Fig. 2i–l and Extended Data Fig. 3d). We observed no significant differences in the percentages of phospho-histone $H3^+$ or $TUNEL^+$ cells in the RV and OFT of mutants when compared to littermate controls (Extended Data Fig. 3e). Lineage tracing experiments demonstrated that RV CMs are specified from CPCs lacking BRD4 (Extended Data Fig. 3a,f).

Fate mapping studies have demonstrated that *Isl1*-expressing progenitors contribute broadly to the adult heart, including the OFT, most of the RV and portions of the inflow pole[24,28]. To test if the observed phenotypes resulted from BRD4 deletion specifically in the anterior compartment of the SHF, we used a second mouse line in which Cre recombinase expression is driven by an anterior heart field (AHF)-specific enhancer of the *Mef2c* gene (*Mef2c-AHF-Cre*)[29]. This allele is expressed slightly later than *Isl1-Cre* and is more restricted to the progenitors that differentiate into cells of the OFT, RV and interventricular septum[29]. Similar to the $Isl1^{Cre}$-*Brd4* analysis, *Mef2c-AHF-Cre*;$Brd4^{flox/flox}$ mutant embryos demonstrated late-gestation lethality between E18.5 (n = 65 embryos; 13 observed versus 16.25 expected; $\chi^2 = 1.65$; $P < 0.05$) and P0 (n = 150 pups; nine observed versus 37.5 expected; $\chi^2 = 32.29$; $P > 0.05$), with the rare mutant animals that survived to birth dying shortly thereafter. At mid-gestational timepoints, *Mef2c-AHF-Cre*;$Brd4^{flox/flox}$ mutant embryos recapitulated the RV hypoplasia phenotype observed in $Isl1^{Cre/+}$;$Brd4^{flox/flox}$ animals when compared with littermate controls (E13.5, 42.3 μm versus 18.0 μm, n = 3, $P < 0.0001$; Fig. 3a,b and Extended Data Fig. 4a). Immunohistochemical assessment of proliferation and apoptosis in the RV and OFT demonstrated minimal differences between mutants and littermate controls (Extended Data Fig. 4b). Although *Mef2c-AHF-Cre*;$Brd4^{flox/flox}$ mutant embryos demonstrated efficient BRD4 deletion in SHF derivatives at early gestational timepoints, (Fig. 3c,d), they were grossly indistinguishable from their littermate controls (Fig. 3e,f; Extended Data Fig. 4c,d), likely due to the later onset and more restricted expression pattern of this Cre allele.

As BRD4 functions as a transcriptional co-activator, we sought to gain molecular insights into the role of BRD4 in SHF CPCs *in vivo* by performing bulk transcriptomic analyses from microdissected SHF derivatives (Extended Data Fig. 5a, red outline) in E9.5 mutant ($Isl1^{Cre/+}$;$Brd4^{flox/flox}$) and control ($Isl1^{Cre/+}$;$Brd4^{flox/+}$) littermate embryos (n ≥ 3 replicates). Principal component analysis (PCA) demonstrated separation of samples according to genotype (Extended Data Fig. 5b), with 2,895 differentially expressed genes, including cardiac transcription factors and structural genes (1,592 downregulated and 1,303 upregulated, log 2 FC ≥ |1|, adjusted $P < 0.05$) (Fig. 4a, Extended Data Fig. 5c and Supplementary Table 2). GO analyses of downregulated genes showed an enrichment for terms related to muscle structure/contraction and mitochondrial biogenesis (Fig. 4b), consistent with the transcriptional consequences of BRD4 deletion at the CPC stage during *in vitro* mESC differentiation (Extended Data Fig. 2g). Among those genes upregulated

after BRD4 deletion GO analyses revealed heterogeneous terms, including several related to transcriptional regulation (Fig. 4b). However, we found that β-catenin-TCF complex assembly and β-catenin-TCF complex were enriched biological process and cellular component GO terms, and the Wnt signaling pathway was the most enriched PANTHER pathway (Fig. 4b,c). Accordingly, multiple genes involved in Wnt signaling, including *Gsk3b*, *Nfatc2* and *Crebbp*, were upregulated in *Isl1*$^{Cre/+}$;*Brd4*$^{flox/flox}$ microdissected SHF tissue when compared to *Isl1*$^{Cre/+}$;*Brd4*$^{flox/+}$ controls (Fig. 4c). Other BET family members were not differentially expressed upon BRD4 deletion (Supplementary Table 2).

BRD4 loss results in excessive Wnt signaling in SHF CPCs *in vivo*

Canonical Wnt signaling promotes CPC maintence[30] and its downregulation in the murine OFT at E9.5 facilitates CM commitment and differentiation[27,31]. As our transcriptomic analyses demonstrated an upregulation of genes involved in Wnt signaling in BRD4 mutants (*Isl1*$^{Cre/+}$;*Brd4*$^{flox/flox}$) versus littermate controls (*Isl1*$^{Cre/+}$;*Brd4*$^{flox/+}$), we performed immunohistochemistry for ISL1, which marks CPCs and is a known target of Wnt signaling[32], at E9.5. Control embryos (*Brd4*$^{flox/flox}$) demonstrated a restricted domain of ISL1-expressing cells in the pharyngeal mesoderm posterior to the OFT, whereas mutant embryos (*Isl1*$^{Cre/+}$;*Brd4*$^{flox/flox}$) had expanded ISL1 expression extending into the OFT and RV (Extended Data Fig. 5d,e). Accordingly, we detected an expansion of AXIN2 (an established downstream target of active Wnt signaling[33]) expressing cells in the same regions of the OFT and RV (Extended Data Fig. 5f,g,n,o). We also observed an increase in the number of ISL1-expressing cells upon JQ1 treatment at the CPC stage during *in vitro* mESC to CM differentiation (Extended Data Fig. 5p,q). *Isl1* expression increased in a dose-dependent manner with JQ1 treatment at the CPC stage in mESC to CM differentiation (Extended Data Fig. 5r). *Mef2c-AHF-Cre;Brd4*$^{flox/flox}$ embryos similarly showed expansion of ISL1 and AXIN2 expressing cells into the OFT and extending to the RV compared to control embryos (Extended Data Fig. 5h–m,s,t).

To assess potential functional relevance of the observed increased Wnt signaling upon JQ1 treatment, which is recapitulated with BRD4 deletion, we concomitantly treated *CMV-CreERT2*;*Brd4*$^{flox/flox}$ mESC-derived CPCs with TAM or VEH and either normal or double the concentration of the Wnt inhibitor XAV939. Increasing XAV939 concentration induced a partial normalization of *Isl1* and related progenitor gene expression (Extended Data Fig. 6a) and TNNT2 staining (Extended Data Fig. 6b–e) when compared to controls. Treatment of hiPSC-derived CPCs with the Wnt inhibitor IWP4 also partially normalized the decrease in TNNT2^{+} CMs induced by JQ1 treatment (Extended Data Fig. 6f,g). These data suggest that the elevated Wnt signaling identified in BRD4 mutant embryos contributes to the observed attenuation of CM differentiation.

To better understand the mechanism underlying the observed increase in Wnt signaling after BRD4 deletion in CPCs, we assessed genome-wide BRD4 occupancy in hiPSC-derived CPCs. Because BRD4 could be acting as either a co-activator or a co-repressor in this context, we also assessed regions of chromatin enriched in trimethylation on lysine 4 of histone H3 (H3K4Me3) and trimethylation on lysine 27 of histone H3 (H3K27Me3), associated with active promoters and regions of transcriptional repression, respectively. We

performed Cleavage Under Targets and Release Using Nuclease (CUT&RUN) for BRD4, FLAG, H3K27Me3 and H3K4Me3 (Fig. 5 and Extended Data Fig. 7) in hiPSC-derived CPCs in duplicate, including a novel cell line in which we biallelically appended a 3×FLAG epitope tag at the N-terminus of BRD4 that we confirmed was karyotypically normal (Extended Data Fig. 7a–c). We first confirmed high replicability between duplicate samples for each condition (Extended Data Fig. 7d) and that FLAG occupancy mirrored that of endogenous BRD4 (Fig. 5a). These data were integrated with published datasets defining genome-wide enrichment of acetylation on lysine 27 of histone H3 (H3K27Ac)[34], a marker of active enhancers, in hiPSC-derived CPCs. BRD4/FLAG peaks demonstrated the greatest overlap with H3K4Me3 peaks (61.5%) followed by H3K27Ac peaks (27%), consistent with previous studies showing that BRD4 facilitates transcriptional activation. We observed nearly no overlap of BRD4/FLAG and H3K27Me3 peaks (1.4%) (Fig. 5b). BRD4/FLAG occupancy was identified in CPCs at candidate Wnt targets, including *AXIN2*, *CCND1*, *ISL1* and *CTNNB1*, as well as at a subset of CM genes, such as *TNNT2* (Fig. 5c,d and Extended Data Fig. 7e–g). Unbiased analysis of BRD4/FLAG occupancy in hiPSC-derived CPCs demonstrated greater enrichment surrounding the transcription start site (TSS) of those genes comprising GO terms associated with Wnt signaling when compared to GO terms associated with contractility (Fig. 5e). Given that BRD4 was found at regions associated with gene activation (H3K4Me3 and H3K27Ac) but not repression (H3K27Me3), our data strongly suggest that BRD4 primarily acts as a co-activator and not as a repressor at the CPC stage. We, therefore, infer that the excessive Wnt signaling observed in mutant embryos upon BRD4 SHF deletion is an indirect effect associated with compromised CM differentiation. However, it remained unclear from our bulk transcriptomic results whether all SHF CPCs are equally affected by BRD4 deletion. Intriguingly, fate mapping of BRD4-null SHF CPCs (Extended Data Fig. 3) indicated that some portion of these cells undergo specification and differentiation into CMs despite absence of this essential chromatin regulator, suggesting that specific subsets of SHF CPCs may be uniquely vulnerable to BRD4 loss.

BRD4 loss has a selective effect in a subset of MSX1/2-positive SHF cells

To determine whether BRD4 loss differentially affects defined subsets of CPCs[35,36], we performed single-cell RNA sequencing (scRNA-seq) on the microdissected heart and surrounding mesoderm (n = 2 embryos per genotype) of *Mef2c-AHF-Cre*;*Brd4*$^{flox/flox}$ mutant embryos and littermate controls (*Brd4*$^{flox/flox}$) at E9.5. We used the *Mef2c-AHF-Cre* as the activity of this Cre allele is more restricted to SHF progenitors and allows for avoidance of ISL1 heterozygosity (the *Isl1-Cre* is a knock-in at the endogenous *Isl1* locus) and because *Mef2c-AHF-Cre;Brd4*$^{flox/flox}$ mutant embryos are indistinguishable from their control counterparts (as compared to RV morphology changes in *Isl1*$^{Cre/+}$;*Brd4*$^{flox/flox}$ mutants versus their control littermates; Fig. 3e,f compared to Fig. 2i,j), thus decreasing concerns that findings could be attributable to developmental delay.

We sequenced 38,900 cells to a median depth of 54,000 reads per cell. After standard quality control, normalization and clustering analysis, we analyzed those clusters of cells in which the *Cre* transcript was detected (Extended Data Fig. 8); this comprised 4,640 cells (2,337 from n = 2 control (*Brd4*$^{flox/flox}$) embryos and 2,303 from n = 2 mutant

(*Mef2c-AHF-Cre;Brd4*$^{flox/flox}$) embryos; Fig. 6a,b). These clusters included the anterior heart field (AHF), branchiomeric muscle (BrM), left ventricle septum (LV septum), OFT, RV and a recently described multi-lineage population (MLP) that comprises a bipotential progenitor compartment giving rise to the AHF and BrM[37] (Fig. 6c). We also detected a population of cells ('cluster 0') defined by expression of *Isl1*, *Mef2c, Msx1, Msx2* and *Dlk1,* among several other genes that represent a subset of SHF precursors that likely contributes to morphogenesis of the OFT[38] (Fig. 6c–e). Cells with this identity were specifically expanded after BRD4 conditional deletion (Fig. 6f and Extended Data Fig. 9). We also observed modest dysregulation of *Nnat, Igfbp5, Rgs5, Hand1, Nebl, Ccnd1, Prtg, Des, Acta2, Myl4, Tnni1* and *Trappc6a* in cluster 0 cells (log 2 FC ≥ |0.25|, adjusted $P < 0.05$). We next applied a method for inferring cellular lineages and developmental trajectories to our single-cell expression data using the MLP as the starting cluster. Analysis of control embryos demonstrated two lineages arising from the MLP, both traveling through cluster 0 and the AHF and giving rise to either BrM or OFT, RV and LV septum (Fig. 6g). Mutant (*Mef2c-AHF-Cre;Brd4*$^{flox/flox}$) embryos demonstrated these same two lineages, along with the emergence of a third predicted lineage arising from the MLP that travels through the AHF and terminates in cluster 0 (Fig. 6h). MSX1/2^{+} cells have been identified in the distal OFT of E9.5-E10.5 embryos[38] in a location corresponding to ISL1^{+} and Wnt^{high} SHF progenitors, and we found an increase in the MSX1/2 expression domain at E9.5–10.5 in BRD4 mutant embryos when compared to controls (Extended Data Fig. 10a–k). Previous studies in craniofacial development and cardiac differentiation indicate that active Wnt signaling promotes *MSX1/2* expression[39,40]. Consistent with these findings, we observed an increase in *Msx1/2* expression in our mESC to CM differentiation assays upon BRD4 deletion, which normalized upon Wnt inhibition (Extended Data Fig. 6a). These data suggest that *Brd4* deletion in the lineage marked by *Mef2c-AHF-Cre* disrupts a subset of distal OFT cells, maintaining them in a less differentiated state.

Discussion

In this study, we performed a CRISPR-based screen to identify genes that can promote or inhibit differentiation of hiPSCs to CMs. This led to discovery of BRD4 as a previously unrecognized regulator of CM differentiation, a finding that we subsequently probed in greater depth *in vitro* and *in vivo* using complementary chemical and genetic approaches. Collectively, our findings highlight a role for BRD4 in controlling cardiac development and add to a growing number of examples that highlight a greater degree of heterogeneity among progenitor populations than was previously appreciated. Several aspects of the BRD4 deletion phenotype can be recapitulated by small-molecule BET BD inhibitors, suggesting that the acetyl-lysine binding activity of BRD4 is important for its role in CPC differentiation and cardiogenesis, but additional targeted structure-function studies are likely to yield important insights. It is intriguing that our previous work identified GATA4 as a BRD4 interacting partner, although this interaction occurs in a BD-independent fashion[25,41]. Future work aimed at defining the BD-dependent binding partners of BRD4 in CPCs will be important for further delineating the mechanistic basis for the phenotypes reported here.

BET BD inhibitors have emerged as promising potential therapies for a number of chronic conditions, including cancer and cardiovascular disease[19,42]. These compounds all share a

structural motif that reversibly binds the BDs of all BET family members, thereby displacing them from their endogenous binding partners. BRD2, BRD3 and BRD4 are ubiquitously expressed, yet no studies explore tissue-specific functions of BRD2 and BRD3 *in vivo,* and only a few examine BRD4 (refs. [22,25,43]). In the contexts where BRD4 has been explored in developmental cell populations *in vivo*, its roles are varied[22,43]. BRD4 deletion in hematopoietic stem cells (HSCs) obliterates HSC development, whereas its deletion in developing resident macrophages results in a more modest compromise of their development and proliferation[43]. Similar to BRD4 deletion in HSCs, BRD4 deletion in progenitor cells of brown adipose tissue (BAT) and muscle lineages results in a severe reduction of BAT and muscle mass along with a failure to induce lineage-specific gene identity programs[22]. In fully differentiated adipocytes, however, BRD4 deletion is largely dispensable for adipose tissue-related gene expression programs[22]. This lies in contrast to roles for BRD4 in both differentiation of a subset of CPCs that we have detailed in the current study as well as in maintenance of metabolic homeostasis in differentiated CMs as we previously described[25]. However, in the present study, we show that progenitor differentiation is also required. Whether other BET proteins can compensate for BRD4 loss in some developmental contexts will be an interesting area for future study.

Our studies also highlight another potential link for how human genetic variation in BRD4 may be related to CHD. *BRD4* mutations have been identified in patients with a Cornelia de Lange-like syndrome (CdLS)[6], a multi-system neurodevelopmental disorder that can include cardiac pathologies (septal defects, outflow obstruction, and vascular anomalies[44]). In one study, two of the three patients with CdLS with predicted pathogenic mutations in *BRD4* had ventricular septal defects[6]. Our study also identifies a subpopulation of MSX1/2-expressing SHF CPCs as particularly sensitive to BRD4 loss. Genetic studies in the Chinese Han population identified single-nucleotide polymorphisms (SNPs) in the *MSX1* gene associated with CHD[45], and a genome-wide association study in European patients with CHD identified a SNP associated with septal defects that was adjacent to and proposed to influence *MSX1* expression[46], suggesting that this cellular subpopulation may play a role in human cardiac development, although the significance of these SNPs remains unknown.

Advances in scRNA-seq have allowed us to uncover heterogeneity in developmental contexts. In particular, these *in vivo* studies have revealed a much earlier segregation of progenitors into distinct committed lineages[36], how dysregulation of specific cellular subpopulations can result in organ-level anatomic defects[4], the temporal and spatial order in which different cardiac lineages arise within the primitive streak[47] and have identified novel progenitor populations[37]. Collectively, the application of scRNA-seq in these studies reveals a far more elaborate map for the sources of cells that form the heart and how perturbations in specific subpopulations can have consequences for organogenesis. Our findings in the context of a differential sensitivity to BRD4 loss in SHF cells, particularly those that express MSX1/2, add to this growing literature. MSX1 and MSX2 are expressed in the distal OFT at E10.5 (ref. [48]) and mark a subset of SHF precursors[38]. Additional experiments investigating why this particular population of cells is so sensitive to BRD4 loss will be of interest. More broadly, future studies aimed at uncovering the cues that pattern these different populations will be an exciting area of investigation with implications for developing *in vitro* methods to produce specific cardiac populations from pluripotent stem cells.

Finally, although we focused on BRD4 in this study, additional efforts may shed light on other hits identified in this and similar screens. Our findings from the integration of these hits with human genetics data from CHD and non-CHD patients support the contention that *in vitro* screens of this nature can have relevance to efforts aimed at understanding the molecular underpinnings of CHD and can aid in prioritizing hits for further study. However, it is important to outline limitations that should be considered when interpreting the genes that were identified. First, our CRISPR-mediated targeting was performed at the hiPSC stage; thus, in the depletion analysis, genes that are critical for hiPSC survival may be identified as potential hits but not have any relevance to CM differentiation. Second, as we used CRISPR-mediated targeting as opposed to CRISPR interference approaches[49], our screening method does not offer fidelity in the context of the specific genetic modifications that are introduced, which may result in variable decreases in target gene expression. Third, as hits identified from our screen could affect any step in hiPSC to CM differentiation, further interrogation of candidates must be performed at the specific stage(s) of interest. Finally, our screen, similar to many others, relied on a readout of guide RNA (gRNA) expression from bulk sequencing of cells in pre-CM and post-CM differentiation conditions, which also limits the sensitivity of our platform. Despite these limitations, the hits identified in our screen will serve as an exciting dataset for hypothesis generation with the potential not only to improve the efficiency of CM differentiation but also to generate novel biological insights into this process.

Methods

Animals

All animal studies were performed in compliance with all relevant ethical regulations in the animal use protocols approved by the Institutional Animal Care and Use Committee of the University of California, San Francisco, and the University of Pennsylvania, following guidelines described in the National Institutes of Health Guide for the Care and Use of Laboratory Animals. The *Brd4*^{flox}, *Isl*^{Cre}, *Mef2c-AHF-Cre* and *R26*^{mTmG} alleles were described previously[22,24,25,29,50]. Mice were maintained on mixed CD1;C57BL/6;129S1/SvImJ genetic backgrounds. Timed matings between male and female mice were set up such that 12:00 on the day of plug detection was considered E0.5. Pregnant females were identified by ultrasound evaluation at E6.5 and euthanized to harvest embryos at E9.5 for scRNA-seq and at E9.5, E10.5, E12.5, E13.5, and E14.5 for histologic evaluation. For scRNA-seq experiments, transcriptomes from at least two embryos were collected per genotype. Embryos were developmentally matched at each time-point by somite count. Animals were housed in AAALAC-accredited facilities where the temperature was set to 72 °C (range, 68–76 °C), and humidity ranged from 30% to 70%, depending on the time of the year, under a 12-h light/dark cycle in same-sex groups of no more than five animals per cage.

Cell lines

HEK293T cells were obtained from the American Type Culture Collection (ATCC); SV20 wild-type hiPSCs were obtained from the University of Pennsylvania iPSC Core Facility[51]; IPSL1 hiPSCs were obtained from Eric Adler (University of California, San Diego); WTC11

hiPSCs (Coriell, GM25256) were obtained from the Gladstone Institutes Stem Cell Core[52]; and D3 mESCs were obtained from the ATCC (CRL-1934).

CM differentiation

Embryonic stem cells (ESCs) were derived from *CMV-CreERT2; Brd4*$^{flox/flox}$ mice as previously described by our group[27,53,54]. In brief, blastocysts were collected at E3.5 and cultured on STO feeder cells in standard ESC media with leukemia inhibitory factor (LIF) and 50 μM MEK1 inhibitor (Cell Signaling Technology, 9900) for 7 d until the blastocysts hatched and colonies formed. Individual colonies were subcultured for approximately 1 week, after which the MEK1 inhibitor was removed, and cells were passed as a normal ESC line. Cardiac differentiation of these cells and D3 mESCs was adapted from published protocols as previously described by our group and others[27,54–56]. In brief, ESCs were cultured and maintained on a feeder layer of mitotically inactivated mouse embryo fibroblast (MEFs) in DMEM with 15% FBS (Thermo Fisher Scientific, SH3007003) and ESGRO LIF (Sigma-Aldrich, ESG1107). Differentiation through the hanging droplets method was initiated after ESC dissociation and suspension at 5×10^4 cells per milliliter in DMEM with 10% FBS (Atlanta Biologicals, S11550) without LIF in 20-μl drops. Two days after droplet formation, embryoid bodies (EBs) were transferred in suspension onto poly-HEMA-coated dishes. After another 2 d, EBs were plated on gelatin-coated dishes in cardiac differentiation media (StemPro-34 SF medium, Invitrogen, 10639–011) supplemented with 5 ng ml^{-1} VEGF (R&D Systems), 10 ng ml^{-1} bFGF (R&D Systems), 12.5 ng ml^{-1} FGF10 (R&D Systems), 2.5 μM XAV939 (Cayman Chemical, 13596), 1 mM ascorbic acid (Sigma-Aldrich, A4403) and 2 mM GlutaMAX (Invitrogen, 35050–061). Beating cells were visible within 24–48 h. BRD4 knockout in *CMV-CreERT2; Brd4*$^{flox/flox}$ ESCs was performed using TAM (Sigma-Aldrich, T176) dissolved in 100% ethanol. Cells were treated with 1 μg ml^{-1} TAM to delete *Brd4*. To attenuate Wnt signaling in the setting of *Brd4* deletion at the CPC stage, *CMV-CreERT2; Brd4*$^{flox/flox}$ mESCs were treated with XAV939 (Cayman Chemical, 13596) and TAM (Sigma-Aldrich, T176) at day 5 in mESC to CM differentiation. The percentage of TNNT2 area was quantified using ImageJ version 1.53t/FIJI. In brief, autofluorescence and troponin images were separately thresholded using primarily the Percentile or Huang methods (total and TNNT2$^+$, respectively) such that the total or TNNT2$^+$ areas were accurately identified, masked and then automatically quantified using the measurement tool. One autofluorescence image and one troponin image were thresholded using the Triangle and Default methods, respectively.

hiPSC cardiomyocyte differentiations were performed using standard published protocols and as previously described by our group[57,58]. In brief, undifferentiated hiPSCs were detached by a 4-min incubation with Accutase (STEMCELL Technologies, 07920) and seeded onto Geltrex (Life Technologies)-coated plates. To induce cardiac differentiation, hiPSC medium was replaced with RPMI/B27-insulin (RPMI-1640 with 2% B-27 supplement minus insulin, Thermo Fisher Scientific) medium supplemented with 100 ng mL^{-1} recombinant human/mouse/rat activin A (R&D Systems) for 18 h, followed by 5 ng mL^{-1} recombinant human BMP-4 (R&D Systems) and 1 nM CHIR 99021 (Cayman Chemicals) for 48 h. The medium was then exchanged for RPMI/B27–insulin with 1 nM XAV939 (Tocris) for 48 more hours. The medium was then replaced with RPMI/B27–

insulin without supplementary cytokines for 72 h. RPMI-B27 (with insulin) was added every 48–72 h thereafter. Widespread spontaneous beating activity was typically observed 10–12 d after the addition of activin A. hiPSCs for the CRISPR-Cas9 screen were maintained in E8 Flex medium (Life Technologies, A2858501) on Matrigel Growth Factor Reduced Matrix (Corning, 354230)-coated plates and passaged regularly using ReLeSR (STEMCELL Technologies, 05872) and treated with 2 μM thiazovivin (Selleck Chemicals, S1459) during passaging. CM differentiation for the CRISPR screen was performed as previously described[8]. In brief, iPSCs were dissociated with Accutase (Innovative Cell Technologies, AT104) and plated on Matrigel (Corning, 354230)-coated plates. Differentiation was initiated by treating iPSCs with 12 μM CHIR-99021 (Selleck Chemicals, CT99021) in RPMI 1640 with B27 minus insulin (Life Technologies, A1895601) for 24 h. Media was replaced with fresh RPMI with B27 minus insulin for 48 h. Cells were then treated with 2 μM Wnt-C59 (Selleck Chemicals, S7037) in RPMI with B27 minus insulin for 48 h. Media was replaced with fresh RPMI with B27 minus insulin for 48 h. Media was then exchanged every 48 h with RPMI containing B27 Supplement (Life Technologies, 17504044). After 15 days of differentiation media was replaced with RPMI 1640 without glucose (Life Technologies, 11879020) supplemented with B27 and 5 mM Lactate (Sigma Aldrich, L7900) to select for differentiated CMs. Lactate selection media was exchanged every 48 h for 10 d. To attenuate Wnt signaling in the setting of pharmacologic BET inhibition at the CPC stage, hiPSCs were treated with IWP4 (5 μM for low dose and 10 μM high dose; Tocris, 5214) concomitant with BET inhibition using JQ1 (25 nM for low dose and 50 nM for high dose; gift from Jun Qi) at day 6 in hiPSC to CM differentiation.

Flow cytometry

mES-derived cells were fixed, permeabilized, and stained for flow cytometry according to standard protocols. In brief, cells were dissociated in 1 mg ml^{-1} collagenase solution, fixed in fixation buffer (eBioscience, 00–8222-49), permeabilized in 1x permeabilization buffer (eBioscience, 00–8333-56), and stored in 1% BSA. Cells were stained with primary and secondary antibodies for 1 h each in permeabilization buffer, resuspended in flow cytometry buffer (eBioscience, 00–4222-26), and analyzed on a BD Accuri C6+ cytometer and manufacturer's software. Antibody used was mouse anti-cardiac troponin T (1:100, Thermo Fisher Scientific, MS-295-P). hiPS-derived cells were collected from day 6 of CM differentiation by Accutase dissociation (STEMCELL Technologies, 07920). Approximately 1×10^6 cells were fixed using fixation buffer (BD Biosciences, 554655), washed two times with 1x permeabilization/wash buffer (BD Biosciences, 554723), incubated for 15 min in 1x permeabilization/wash buffer and resuspended in 100 μl of 1x permeabilization/wash buffer supplemented with 1 μl of the appropriate antibody at room temperature for 40 min with gentle rocking. Cells were washed two times in 1 ml of FACS buffer (5% FBS, 0.1% NaN3, and 1mM EDTA in 1x PBS) and resuspended in FACS buffer. Cells were analyzed on a BD Fortessa X20 cytometer. Antibody used was BV421-conjugated mouse anti-cardiac troponin T (BD Biosciences, 565618) or isotype control (BD Biosciences, 562439). Flowjo or software provided with the BD Accuri C6+ flow cytometer was used for all FACS data analysis.

‘Brunello’ human CRISPR library amplification

The ‘Brunello’ lenti-CRISPR plasmid library was obtained from Addgene (no. 73178) and was amplified according to established protocols as previously described[8]. In brief, pooled Brunello lenti-CRISPR was introduced into Endura electrocompetent cells (Lucigen, 60242–2) by electroporation. Recovered cells were plated on 500-cm^2 bioassay plates (Corning, 06–443-22) with LB agar containing ampicillin and grown overnight at 30 °C. Cells were pelleted, and DNA was collected using a ZymoPURE Maxiprep Kit (Zymo Research, D4202).

Virus production

Virus was produced in HEK293T cells transduced with lentiviral expression plasmid and pMD2 and psPAX2 lentiviral packaging plasmids. In brief, cells were grown in Opti-MEM (Thermo Fisher Scientific, 31985062) media supplemented with Lipofectamine (Thermo Fisher Scientific, 11668030) and Plus Reagent (Thermo Fisher Scientific, 11514015). Supernatant was collected 60 h after transduction and filter sterilized using a Steriflip filtration device (Millipore Sigma, SE1M003M00).

CRISPR screening, DNA preparation and analysis

The ‘Brunello’ library infection rate was optimized as previously described[8]. hiPSCs were dissociated to a single cell suspension using Accutase and plated at 12.5 million cells per flask into eight T225 flasks (Thermo Fisher Scientific, 159934) with 8 μg mL^{-1} polybrene. ‘Brunello’ lenti-CRISPR virus was added to achieve an infection rate of 30% (600 μL of virus per flask) into seven flasks, leaving one flask uninfected as a control for puromycin selection. After 48 h, infected hiPSCs were dissociated, pooled, and re-plated into five 875 cm^2 multilayer flasks (Falcon, 353144). Uninfected hiPSCs were dissociated and re-plated at a ratio of 1:3 into a T225 flask and, 48 h after passaging, were treated with 0.4 μg ml^{-1} puromycin. Puromycin selection media was exchanged daily until no cells remained in the uninfected control condition for a total of 6 d. When the infected hiPSCs reached 80% confluence, they were passaged for differentiation, and a portion was reserved for DNA collection. Cells were re-plated at a density of 14.5 million cells per T225 flask, and differentiation was performed. Cells reserved for sequencing were pelleted, rinsed with cold PBS, and stored at −20 °C. DNA preparation and analysis were performed as previously described[8]. In brief, the RIGER version 2.0.2 algorithm[59] was used to enrich sgRNAs that promote or inhibit CM differentiation. This non-parametric statistical approach uses a Kolmogorov-Smirnov-based statistic to calculate gene scores with the output of a rank ordered list of genes based on the depletion or enrichment of the sgRNAs that target them.

RNA generation, sequencing, mapping and quantification

ES-derived cellular RNA was isolated in TRIzol (Invitrogen, 15596–026), and RNA was obtained using Qiagen RNeasy spin columns, with on-column DNAse I digestion following the manufacturer’s directions. Similarly, microdissected E9.5 hearts and the pharyngeal mesoderm immediately posterior to the OFT and anterior to the neural tube were isolated into TRIizol, and RNA was obtained using Qiagen RNeasy spin columns, with on-column DNAse I digestion following the manufacturer’s directions. Complementary DNA (cDNA)

was synthesized according to kit instructions with the SuperScript III system (Invitrogen). Quantitative RT-PCR was performed in at least three biological replicates using SYBR Green (Applied Biosystems). *Gapdh* and *HPRT* were used as a reference control gene for murine and human studies, respectively. Quantitative RT-PCR data presented as 'Relative gene expression' describe FC of treatment versus control samples. Quantitative RT-PCR primer sequences are available upon request. For RNA-seq, replicate RNA sample quality was analyzed by a Bioanalyzer (Agilent Genomics) with the RNA 6000 Nano assay; samples with RNA integrity number (RIN) scores greater than 8 were chosen for library construction. Bulk RNA libraries were prepared using the NEBNext Ultra II DNA Library Prep Kit (New England Biolabs (NEB)) with the NEBNext Poly(A) mRNA Magnetic Isolation Module (NEB) to enrich poly(A)-tailed RNA molecules. Libraries were PCR amplified with single-end barcodes using Illumina Multiplex Oligos (NEB). RNA-seq library quality was analyzed by Bioanalyzer (Agilent Genomics), and libraries were individually quantified using qPCR (Kapa Biosystems). Libraries were pooled for multiplex sequencing and re-quantified by qPCR (Kapa Biosystems), and the final pool was sequenced on the Illumina NextSeq 500 platform (version 2; 75-bp single-end sequencing, high output, Illumina).

Differential gene expression and pathway enrichment analysis

Bulk RNA-seq raw reads were trimmed with Trimmomatic version 0.32, aligned to the mm10 genome using STAR[60] (version 2.6.0c) and then filtered using SAMtools view with '-F 4 -q 10' parameters. Rsubread[61] featureCounts was used to quantify the number of reads per feature of the Ensembl mm10 gene annotation file. For differential gene expression analysis, genes with fewer than 1 count per million (CPM) in less than 25% of samples were removed from differential expression analysis. For analyses using all genes, no CPM filter was applied. EdgeR[62,63] calcNormFactors was used to calculate library size normalization factors. The Limma voom function was used to $\log_2$ transform and quantile normalize the CPM matrix. Gene count data were processed to $\log_2$ CPM using the Bioconductor package edgeR version 3.32.1. Samples underwent PCA to assess replicate similarity via PCA clustering. Replicates that did not group tightly with their respective samples were excluded. Differential gene expression analysis was performed using Limma version 3.46.0, and Gene Ontology (GO) enrichment analysis was performed using topGO 2.42.0 in R version 4.0.5. Sequencing and count data were deposited into the Gene Expression Omnibus with the accession number: GSE184922.

Embryo dissection and single-cell library generation/sequencing

The entire cardiogenic region was dissected including the SHF region as previously described[4]. Due to the small size of embryos at these stages, some surrounding tissue was microdissected to ensure complete retrieval of cardiac populations. Embryos were dissected in cold PBS (Life Technologies, 14190250), de-yolked and placed in PBS with 1% FBS (Thermo Fisher Scientific, 10439016) solution on ice until dissociation (approximately 3 h). Yolk sac DNA was extracted (QuickExtract DNA Extraction Solution, Epicentre, QE09050) and used for genotyping before further microdissection of cardiac regions at each stage. Dissected cardiac tissue was incubated in 200 μl of TrypLE (Thermo Fisher Scientific, 12563029) for 5 min, triturated with a 200-μl pipette tip and incubated for an additional

5 min. The TrypLE solution was quenched with 600 μl of PBS with 1% FBS. Cells were filtered through a 70-μm cell strainer (BD Falcon, 08–771-2), centrifuged at 150g for 3 min, and resuspended in 35 μl of PBS with 1% FBS. Single-cell droplet libraries from this suspension were generated in the 10x Genomics Chromium controller according to the manufacturer's instructions in the Chromium Single Cell 3′ Reagent Kit version 3 User Guide. Additional components used for library preparation include the Chromium Single Cell 3′ Library and Gel Bead Kit version 3.0 (PN-1000121) and the Chromium Single Cell 3′ Chip Kit version 3.0 (PN-1000127). Final libraries were pooled and sequenced in the same lane on a HiSeq 4000 or NextSeq 500. All libraries were sequenced to a mean read depth of at least 50,000 total aligned reads per cell.

Processing of raw sequencing reads

Raw sequencing reads were processed using the Cell Ranger version 3.0.2 pipeline from 10x Genomics. In brief, reads were demultiplexed and aligned to the mouse mm10 genome that was modified to include a Cre sequence, and unique molecular identifier (UMI) counts were quantified per gene per cell to generate a gene-barcode matrix. Data from multiple samples were aggregated and normalized to the same sequencing depth, resulting in a combined gene-barcode matrix of all samples.

Cell filtering and cell-type clustering analysis

The transcriptomes of 39,000 cells were sequenced to a median depth of 54,000 reads per cell. Filtering, quality control, normalization, and clustering analyses of these cells were performed with the Seurat version 3 R package[64], as described previously[4]. Low-quality or doublet-encapsulated cells were excluded by filtering out cells with raw UMI counts between 5,000 and 75,000, and fewer than 7,500 genes. Additionally, cells with over 15% of reads aligning to the mitochondrial genome, an indicator of unhealthy or dying cells, were excluded. Regression was used to eliminate technical variability due to the number of genes detected and cell cycle stage. Significant principal components (PCs) were used for downstream graph-based, semi-unsupervised clustering into distinct populations, and uniform manifold approximation and projection (UMAP) dimensionality reduction was used to project these populations in a two-dimensional plot. Endoderm-derived, ectoderm-derived, and mesoderm-derived clusters were identified using markers of each lineage and retained the mesoderm clusters in which Cre expression was detected (AHF populations). The retained cells had 20,000 median UMIs per cell, corresponding to a median of 4,700 genes. Cells with left ventricular identity were also retained due to their high transcriptional similarity with right ventricular cells[4]. The regression, PC selection, clustering, and UMAP projection were then repeated for these retained populations. To identify marker genes, the resulting clusters were compared pairwise for differential gene expression using the Wilcoxon rank-sum test for single-cell gene expression (*FindAllMarkers* function). An adjusted P value (Bonferroni correction) cutoff of less than 1×10^{-4} was used to identify differentially expressed genes between *Brd4*$^{flox/flox}$ and *Mef2c-AHF-Cre*; *Brde4*$^{flox/flox}$ cells (*FindMarkers* function) within each population. Pseudotime analysis was performed using the Slingshot version 2.6.0 R library[65]. Embeddings and cluster labels from the analysis Seurat object were passed to Slingshot's getLineages() function, which was run with standard settings aside from the 'start.clus' parameter, which was set to begin

pseudotime from the multi lineage population (MLP) cluster. Resultant lineages were passed to Slingshot's getCurves() function to finalize computation pseudotime lineages (approx_points = 300, thresh = 0.01, stretch = 0.8, allow.breaks = FALSE, shrink = 0.99). Pseudotime plots were generated using base R and ggplot2 libraries. R scripts are available upon request.

Generation of BRD4^{FLAG} hiPSC line

The *BRD4*$^{FLAG/FLAG}$ hiPSC line was generated in WTC11 cells[52] as previously described[41]. In brief, WTC11 hiPSCs were dissociated in Accutase (STEMCELL Technologies, 07920), and 250,000-cell aliquots per condition were nucleofected with Cas9-ribonucleoprotein (Cas9-RNP) complexes with a homology-directed repair (HDR) template following the Primary Cell Nucleofection Kit manufacturer's instructions (Lonza, V4XP-3960). The synthetic guide RNAs (sgRNAs) targeting the N-terminus of the ATG-containing exon of BRD4 were hBRD4_gRNA-16 (GTGCCTGGTGAAGAATGTGA) and hBRD4_gRNA+8 (ACTAGCATGTCTGCGGAGAG). An HDR template introducing a 3×FLAG epitope and GGGS linker was ordered as an Alt-R HDR Donor Oligo from Integrated DNA Technologies (GGGGCTCTTCTCTTCCTTTGTAGAGTGCCTGGTGAAGAATGTGATGAGATCACTAGCATGGACTACAAAGACCATGACGGTGATTATAAAGATCATGATATCGATTACAAGGATGACGATGACAAGGGTGGTGGTGGTTCTTCTGCGGAGAGCGGCCCTGGGACGAGATTGAGAAATCTGCCAGTAATGGGGGATGGACT). Colony picking followed by clone screening for biallelic insertion of the 3×FLAG and linker sequences was performed by PCR (hBRD4_tagged_F: 5′-GTGCCCATCTGCTGACTGAT-3′; hBRD4_tagged_R: 5′-TTGAGCACCACTCTGAGCAG-3′) generating a wild-type product of 300 bp and a knock-in product of 381 bp. Targeted knock-in was confirmed by Sanger sequencing, and the final monoclonal cell lines were checked for normal karyotype (Cell Line Genetics).

CUT&RUN chromatin profiling

CUT&RUN was performed as previously described by our group[26] with slight modifications as per a commercially available CUT&RUN kit (EpiCypher, 14–1048). Antibodies used were mouse anti-FLAG (Sigma-Aldrich, F1804), rabbit anti-BRD4 (EpiCypher, 13–2003), rabbit anti-H3K4Me3 (EpiCypher, 13–0041), rabbit anti-H3K27Me3 (EpiCypher, 13–0055) and rabbit IgG (EpiCypher, 13–0042). All CUT&RUN data were initially processed using the nfcore CUT&RUN pipeline (nf-core/cutandrun version 2.0 (ref.66)) with standard settings, aligned to hg38. In brief, this pipeline performs data quality control, adapter trimming, sequence alignment, spike-in normalization and preliminary peak calling. To acquire a final set of CUT&RUN peaks, Sparse Enrichment Analysis for CUT&RUN (SEACR) version 1.3 was run outside of the nfcore framework to produce a robust peak set for all samples after applying an FDR threshold of 1×10^{-2} to called peaks, as opposed to calling peaks against IgG controls. bigWig files were post-processed using BEDTools subtract version 2.31.0 to subtract IgG signal from experimental samples. The resultant IgG-subtracted bigWig files were used in all heat maps produced with deepTools computeMatrix and plotHeatmap functions version 3.5.1. Heat map region BED files were produced with R version 4.2.2, where the ChIPseeker version 1.34.1 library was used for peak annotation using the annotatePeak() function when applicable, and the

TxDb.Hsapiens.UCSC.hg38.knownGene version 3.16.0 library was used for retrieval of associated genomic coordinates of transcripts or regions to plot. All scripts are available upon request.

Histology

Embryos were fixed in 2% paraformaldehyde (4 °C overnight), dehydrated through an ethanol series, embedded in paraffin and sectioned. Antibodies used for immunohistochemistry included Brd4 (rabbit, Bethyl, 00396), phospho-histone H3 (rabbit, Cell Siganling Technology, 9701L), Islet1 (mouse, Developmental Studies Hybridoma Bank, 39.4D5), Tnnt2 (mouse, Thermo Fisher Scientific, MS-295P1), Axin2 (rabbit, Abcam, ab32197), MSX1+2 (chicken, Developmental Studies Hybridoma Bank, 4G1), cleaved caspase 3 (rabbit, Cell Signaling Technology, 9664L), GFP (goat, Abcam, ab6673), and RFP (rabbit, Rockland, 600–401-379). Hematoxylin and eosin (H&E) and TUNEL staining were performed using standard protocols. RNAScope was performed according to the manufacturer's instructions (Advanced Cell Diagnostics; Msx2, 421851, Msx1, 421841, Axin2, 400331). Ventricular thickness was manually quantified using the measurement tool in ImageJ version 1.53t/FIJI or Adobe Illustrator at random points along the ventricular wall. Quantification was performed on images of H&E-stained sections save for $Isl1^{Cre/+}$ embryos at the E14 timepoint where TNNT2 immunohistochemistry images were used. Sections were imaged on a Nikon Eclipse 80i fluorescence microscope or a Leica DMi8 inverted fluorescence microscope.

Immunoblotting

Protein lysates were run on 4–12% Bis-Tris protein gels (Invitrogen), and blots were probed with anti-BRD4 (1 μg ml^{-1}, Bethyl, 00396) or anti-β-actin (1:1,000, Cell Signaling Technology, 4967). Anti-rabbit HRP-conjugated secondary antibody (Cell Signaling Technology, 7074) was used at 1:2,500. Visualization was achieved using ECLPrime (GE Life Sciences, RPN2232) or SuperSignal West Femto Chemiluminescent Substrate (Thermo Fisher Scientific, 34094).

Statistics and reproducibility

All statistical comparisons were performed in R version 3.5.2 or GraphPad Prism version 9/version 10, as specified in the relevant figures and corresponding Methods sections. The number of replicates, statistical test used, test result and significance levels are described in each figure legend. When presenting representative results showing histologic analyses of embryos, at least two independent embryos were analyzed. When presenting representative results for immunocytochemistry of mESC-derived tissues, at least three independent differentiations were analyzed.

Extended Data

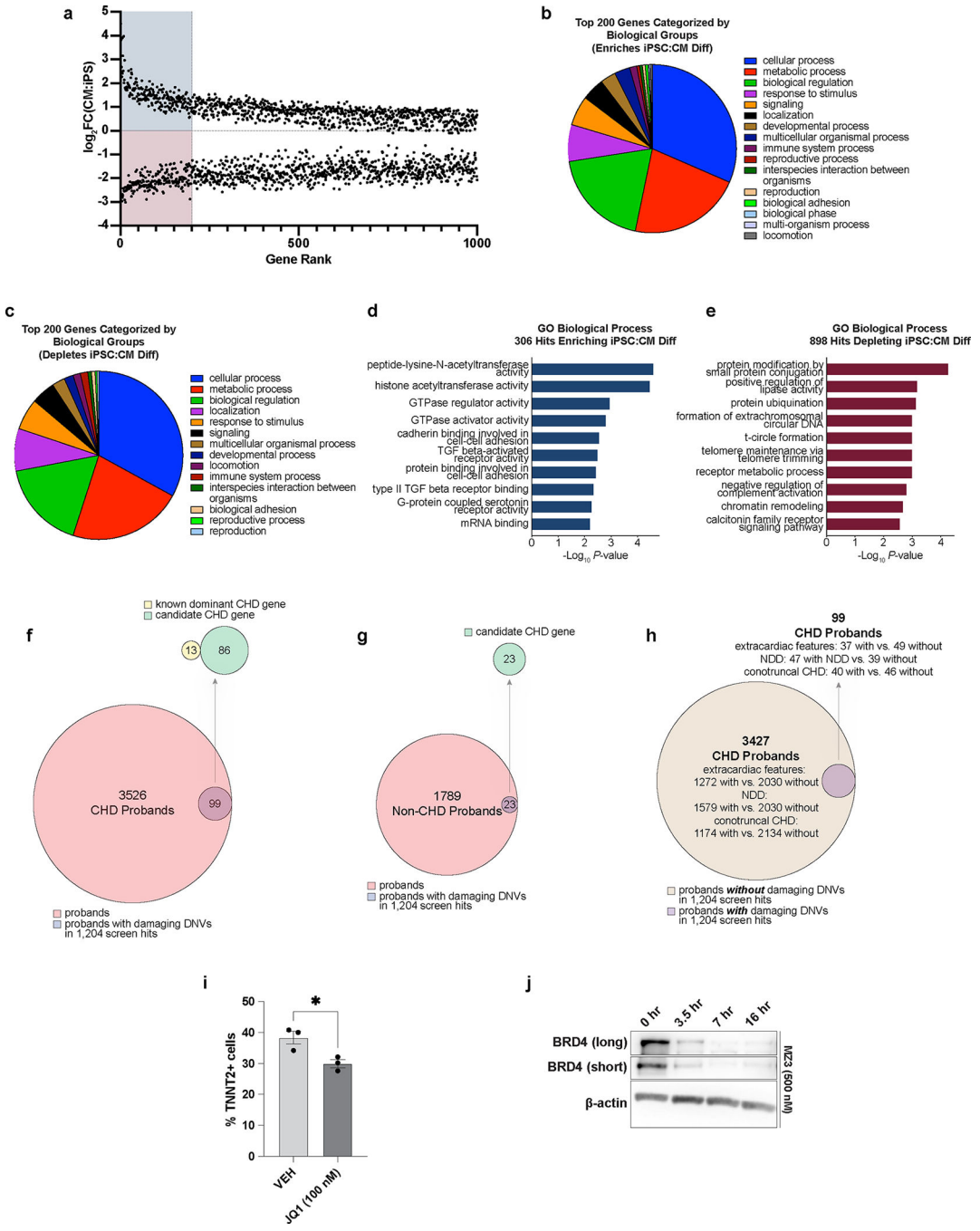

Extended Data Figure 1: Integrating a CM differentiation screen and CHD variants.

(**a**) Top 1000 genes ranked by enrichment or depletion. (**b-c**) Categorization of top 200 genes enriched (b) or depleted (c) in cardiac myocytes compared to undifferentiated hiPSCs by biological groups. (**d-e**) Gene ontology (GO) analysis of top enriched (d) or depleted (e) hits (see Methods for details). (**f-g**) Venn diagrams demonstrating the number of CHD (f) or Non-CHD (g) probands with predicted damaging DNVs in hits identified in

our screen as enriching hiPSC:CM differentiation or depleting hiPSC:CM differentiation. Arrows depict Venn diagrams representing the number of probands from each cohort with predicted damaging DNVs identified in our screen that have mutations in known dominant CHD genes or where these candidate CHD genes may potentially be causative. (**h**) Venn diagram demonstrating the number of CHD probands with (purple) or without (brown) damaging DNVs in hits identified in our screen highlighting no enrichment for extracardiac anomalies (p=0.43) or neurodevelopmental delay (NDD; p=0.23) and a slight enrichment for conotruncal CHD (p=0.04). (**i**) TNNT2+ cells quantified by flow cytometry at day 10 of hiPSC to CM differentiation in WTC11 cells treated with 100nM JQ1 starting at day 6 (n=3 biologically independent samples). (**j**) MZ3 treatment (500 nM for 0, 3.5, 7, and 16 hours) effectively degrades BRD4 in SV20 hiPSCs as assessed by immunoblot analysis for BRD4 with β-actin expression as a loading control. In all graphs, error bars represent ±1 SEM. * represents p=0.0271 (two-tailed unpaired t test).

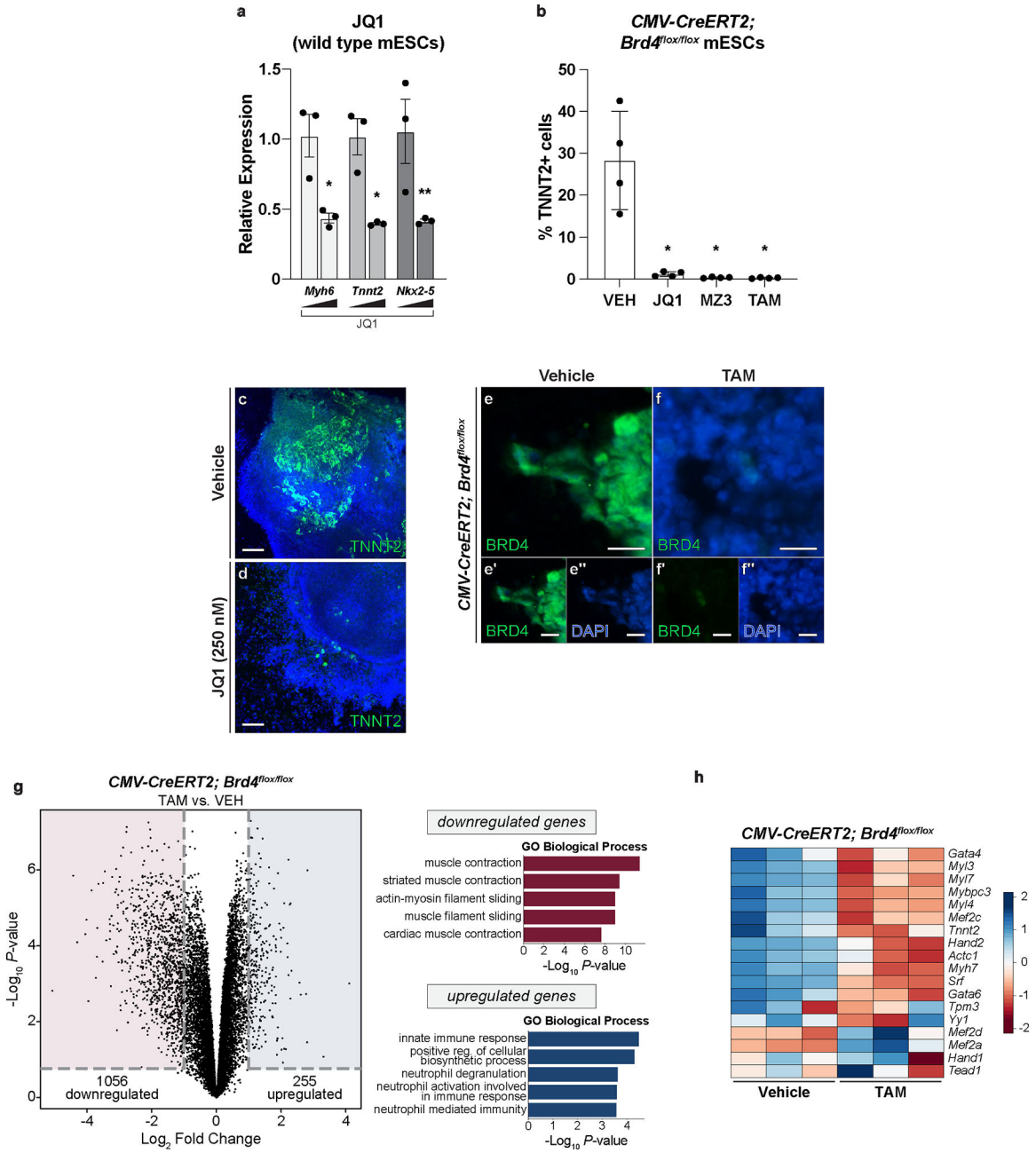

Extended Data Figure 2: tion or deletion of BRD4 inhibits mESC cardiac differentiation.

Inhibi (**a**) Expression of *Myh6*, *Nkx2–5*, and *Tnnt2* at day 7 of mESCs cardiac differentiation treated with JQ1 (100 nM) starting day 5 of differentiation (n=3 biologically independent samples). (**b**) TNNT2+ cells quantified by flow cytometry at d9 of mESC differentiation in *CMV-CreERT2; Brd4*$^{flox/flox}$ cells treated with 4-hydroxytamoxifen (TAM), JQ1 (250 nM) or MZ3 (500 nM) starting at day 5 (n=3 biologically independent samples). (**c-d**) Immunofluorescence of TNNT2 at day 9 of mESC to CM differentiation in wild type cells treated with JQ1 (100 nM) or vehicle starting at day 5. (**e-f**) Immunofluorescence of BRD4 in vehicle (ethanol, e-e′′) and TAM (f-f′′) treated

undifferentiated mESCs. (**g**) Volcano plot showing RNA-seq from *CMV-CreERT2; Brd4$^{flox/flox}$* (TAM vs. vehicle [VEH]) mESCs and gene ontology analysis of downregulated and upregulated genes (see Methods for details). (**h**) Heatmap showing expression of select transcription factor and muscle structural protein genes from RNA-seq in *CMV-CreERT2; Brd4$^{flox/flox}$* (TAM vs. VEH) mESC-derived cardiac tissues (day 10; TAM or VEH added at day 5). In all graphs, error bars represent ±1 SEM. For a, all comparisons are made relative to 0 nM compound for each gene; * represents p<0.0493, ** represents p<0.0085 (two-tailed unpaired t test). For b, all comparisons are made relative to VEH for each condition; * represents p<0.0188 (two-tailed unpaired t test). Scale Bars = 100 μm (c, d, e, e′, e′′, f, f′, f′′)

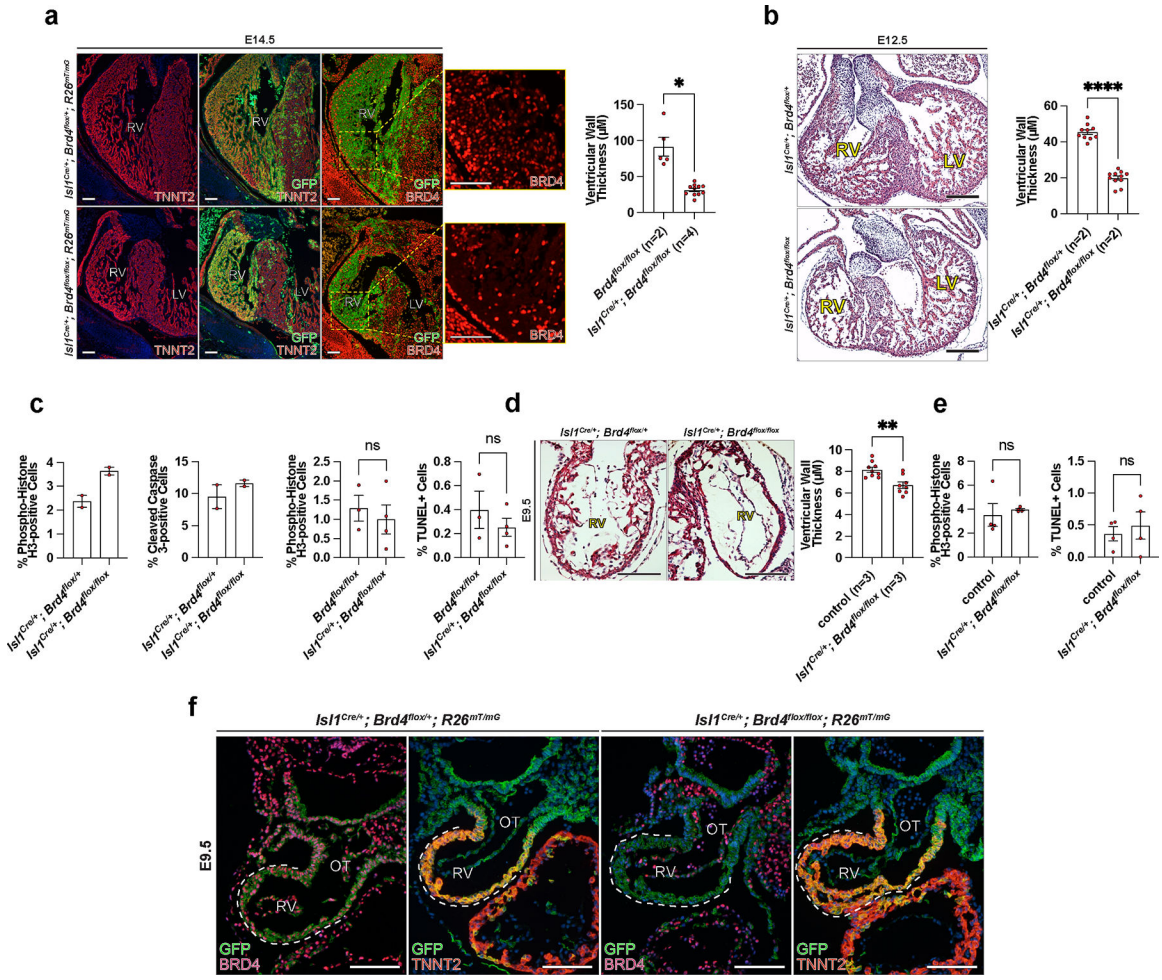

Extended Data Figure 3: Loss of BRD4 in *Isl1^{Cre}*-SHF progenitors *in vivo* results in myocardial hypoplasia.

(**a**) Lineage tracing of *Isl1$^{Cre/+}$*; *Brd4$^{flox/+}$* and *Isl1$^{Cre/+}$*; *Brd4$^{flox/flox}$* with *R26$^{mTmG/+}$* allele. Immunohistochemistry of ISL1-derived cells (GFP) and TNNT2 or BRD4 (red) in heart and quantitative assessment of right ventricular myocardial wall thickness in indicated genotypes at E14 (5 sections from n=2 control embryos and 11 sections from n=4 mutant embryos). (**b**) Hematoxylin and eosin staining of a section through outflow tract and RV of *Isl1$^{Cre/+}$*; *Brd4$^{flox/+}$* and *Isl1$^{Cre/+}$*; *Brd4$^{flox/flox}$* embryos at E12.5 and quantitative assessment of right

ventricular myocardial wall thickness in indicated genotypes (10 sections from n=2 control embryos and 11 sections from n=2 mutant embryos). (**c**) Quantification of percentage phospho-histone H3-, cleaved caspase 3-, and TUNEL-positive cells in the RV of E12.5 and E14.5 embryos of indicated genotypes (n=2 biologically independent samples per genotype at E12.5; n=3–4 biologically independent samples per genotype at E14.5). (**d**) Hematoxylin and eosin staining of a section through outflow tract and RV of *Isl1*$^{Cre/+}$; *Brd4*$^{flox/+}$ and *Isl1*$^{Cre/+}$; *Brd4*$^{flox/flox}$ embryos at E10 and quantitative assessment of right ventricular myocardial wall thickness in indicated genotypes (9 sections from n=3 control embryos and 8 sections from n=3 mutant embryos). (**e**) Quantification of percentage phospho-histone H3- and TUNEL-positive cells in the RV of E10 control (*Isl1*$^{Cre/+}$; *Brd4*$^{flox/+}$ or *Brd4*$^{flox/flox}$) and *Isl1*$^{Cre/+}$; *Brd4*$^{flox/flox}$ embryos (n=4 biologically independent samples per condition). (**f**) BRD4 and TNNT2 immunohistochemistry along with lineage tracing with *R26*$^{mTmG/+}$ allele in *Isl1*$^{Cre/+}$; *Brd4*$^{flox/+}$ and *Isl1*$^{Cre/+}$; *Brd4*$^{flox/flox}$ E9.5 embryos at level of right ventricle. Error bars represent ±1 SEM. All comparisons are made as indicated; * represents p=0.0091, ** represents p=0.0021, **** represents p<0.0001 (two-tailed unpaired t test). RV, right ventricle; LV, left ventricle; OT, outflow tract. Scale Bars = 100 μm (a, b, d, f)

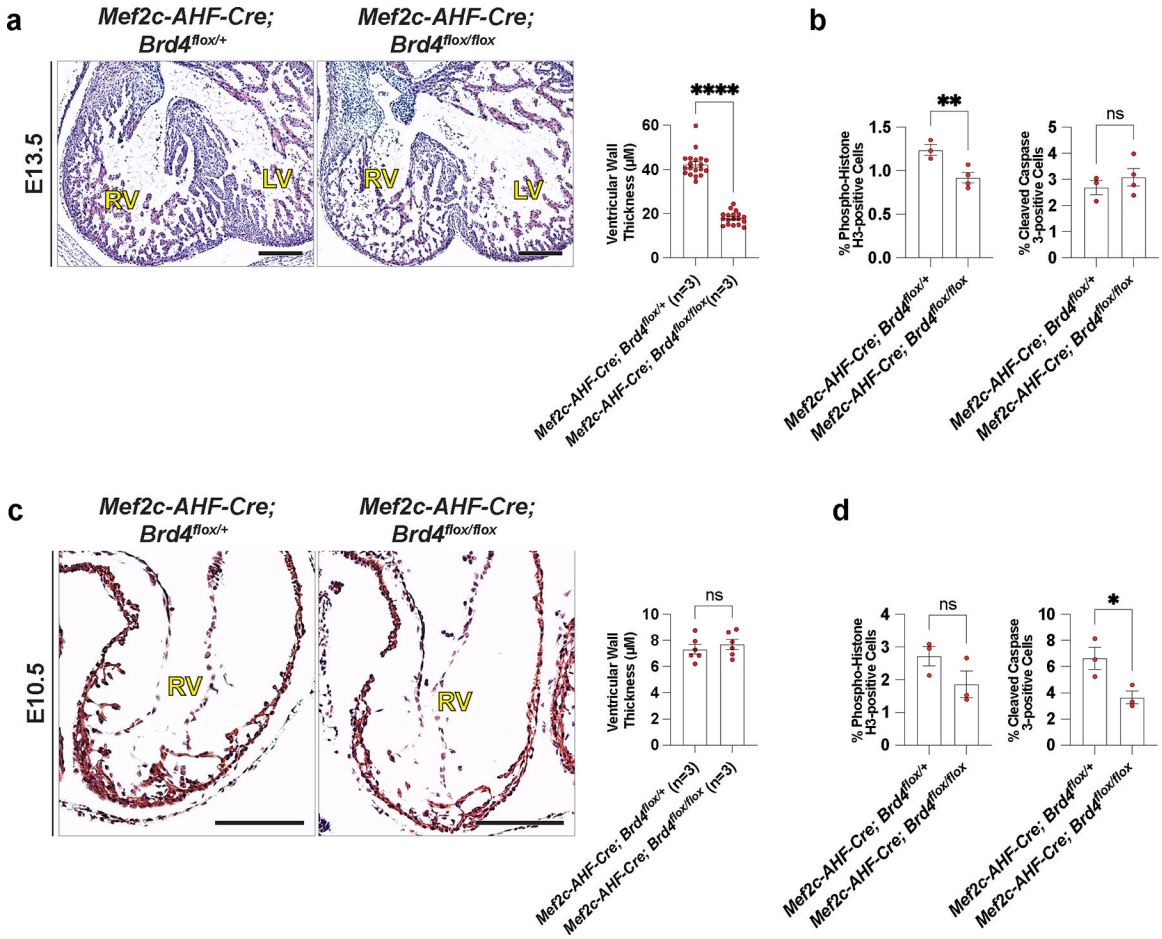

Extended Data Figure 4: Loss of BRD4 in *Mef2c-AHF-Cre*-SHF CPCs *in vivo* results in right ventricular thinning.

(**a**) Hematoxylin and eosin staining of a section through outflow tract and RV of *Mef2c-AHF-Cre*; *Brd4*$^{flox/+}$ and *Mef2c-AHF-Cre*; *Brd4*$^{flox/flox}$ embryos at E13.5 and quantitative assessment of right ventricular myocardial wall thickness in indicated genotypes (19 sections from n=3 control embryos and 18 sections from n=3 mutant embryos). (**b**) Quantification of percentage phospho-histone H3- and cleaved caspase 3-positive cells in the RV of E13.5 *Mef2c-AHF-Cre*; *Brd4*$^{flox/+}$ and *Mef2c-AHF-Cre*; *Brd4*$^{flox/flox}$ embryos (n=3–4 biologically independent samples per genotype). (**c**) Hematoxylin and eosin staining of a section through outflow tract and RV of *Mef2c-AHF-Cre*; *Brd4*$^{flox/+}$ and *Mef2c-AHF-Cre*; *Brd4*$^{flox/flox}$ embryos at E10.5 and quantitative assessment of right ventricular myocardial wall thickness in indicated genotypes (6 sections from n=3 control embryos and 6 sections from n=3 mutant embryos). (**d**) Quantification of percentage phospho-histone H3- and cleaved caspase 3-positive cells in the RV of E10.5 *Mef2c-AHF-Cre*; *Brd4*$^{flox/+}$ and *Mef2c-AHF-Cre*; *Brd4*$^{flox/flox}$ embryos (n=3 biologically independent samples per genotype). Error bars represent ±1 SEM. All comparisons are made as indicated; * represents p=0.0489, ** represents p=0.0146, **** represents p<0.0001 (two-tailed unpaired t test). RV, right ventricle; LV, left ventricle. Scale Bars = 100 μm (a, c).

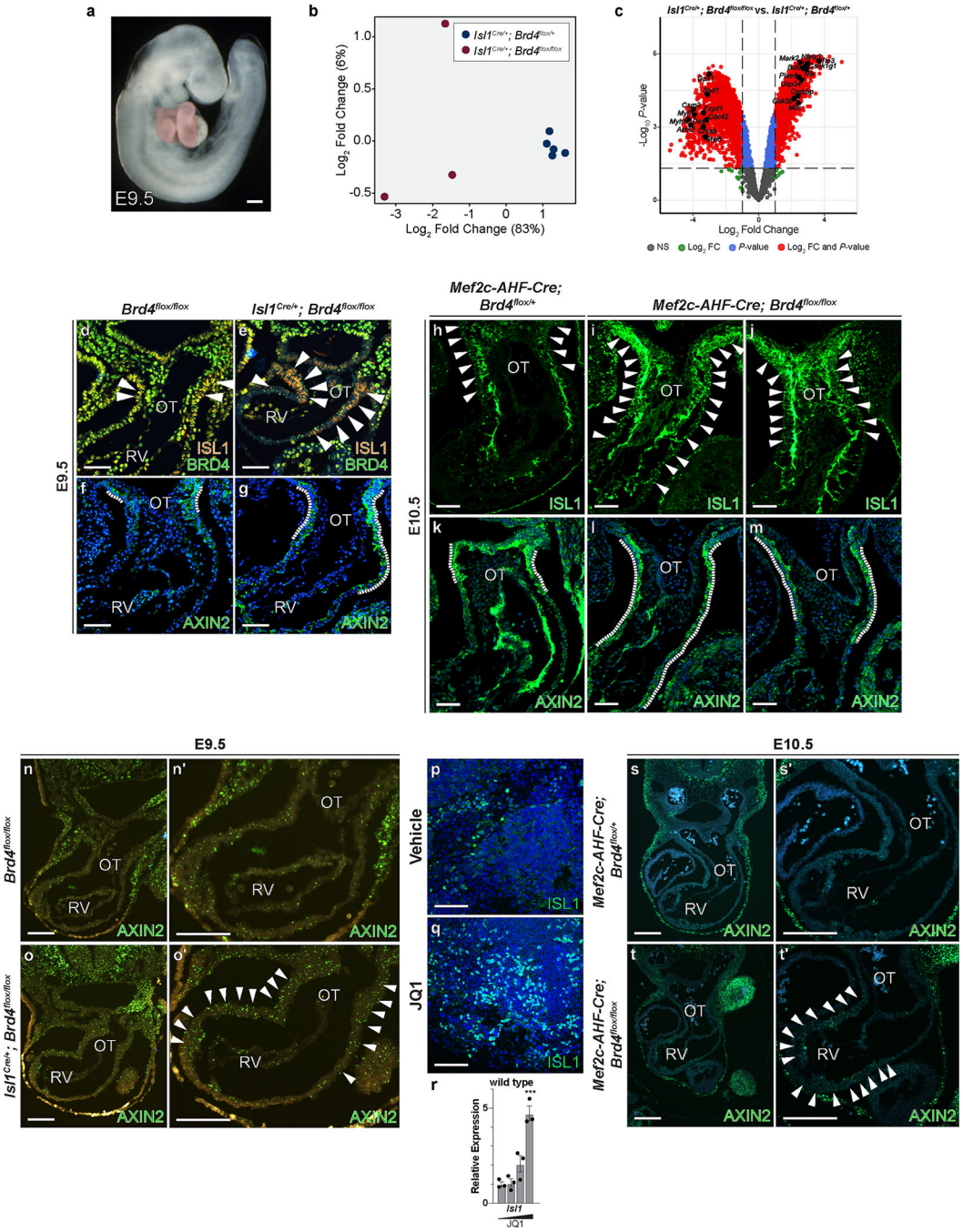

Extended Data Figure 5: Wnt signaling is dysregulated upon BRD4 depletion in CPCs.

(**a**) Image of *Isl1*$^{Cre/+}$; *Brd4*$^{flox/+}$ embryo appearing in Figure 2i with region microdissected for bulk RNA-seq highlighted in red. (**b**) Principal component analysis of RNA-seq from *Isl1*$^{Cre/+}$; *Brd4*$^{flox/+}$ (blue) and *Isl1*$^{Cre/+}$; *Brd4*$^{flox/flox}$ (red) E9.5 embryos. (**c**) Volcano plots of E9.5 *Isl1*$^{Cre/+}$; *Brd4*$^{flox/+}$ vs. *Isl1*$^{Cre/+}$; *Brd4*$^{flox/flox}$ embryonic hearts (same data appearing in Figure 4) with a subset of cardiac and Wnt-related genes annotated (see Methods for details). *Isl1*$^{Cre/+}$; *Brd4*$^{flox/+}$ (**d,f**) and *Isl1*$^{Cre/+}$; *Brd4*$^{flox/flox}$ (**e,g**) E9.5 embryos at level of right ventricle stained with ISL1 (red, d-e), BRD4 (green, d-e), or AXIN2

(green, f-g). Note the expansion of ISL1- (arrow heads) and AXIN2- (dotted line) expressing cells into the RV from distal outflow tract in mutant embryos. (**h-m**) ISL1 and AXIN2 Immunohistochemistry of E10.5 *Mef2c-AHF-Cre*; *Brd4*$^{flox/+}$ (h,k) and *Mef2c-AHF-Cre*; *Brd4*$^{flox/flox}$ (i,j,l,m) embryos at the level of outflow tract. (h-j, ISL1; k-m, AXIN2). Note the expansion of ISL1- (arrow heads) and AXIN2- (dotted line) expressing cells into the right ventricle from distal outflow tract in mutant embryos. (**n-o**) AXIN2 RNAscope of *Brd4*$^{flox/flox}$ (n,n′) and *Isl1*$^{Cre/+}$; *Brd4*$^{flox/flox}$ (o,o′) E9.5 embryos at the level of the right ventricle (n′ and o′ are magnified images of n and o, respectively). (**p-q**) ISL1 representative immunofluorescence at day 8 of mESC-derived cardiac cultures treated with vehicle (DMSO; VEH) (p) or JQ1 (500 nM) (q) starting at day 5. (**r**) *Isl1* expression in day 8–9 mESC-derived cardiac cultures treated with increasing doses of JQ1 (0–500 nM; JQ1 added at day 5; n=3 n=3 biologically independent samples per dose). (**s-t**) AXIN2 RNAscope of *Mef2c-AHF-Cre*; *Brd4*$^{flox/+}$ (s,s′) and *Mef2c-AHF-Cre*; *Brd4*$^{flox/flox}$ (t,t′) E10.5 embryos at level of right ventricle (s′ and t′ are magnified images of s and t, respectively). For r, all comparisons are made relative to 0 nM compound. *** represents p=0.0007 (two-tailed unpaired t test). RV, right ventricle; OT, outflow tract. Scale Bar = 250 μm (a), 50 μm (d-m, n, o, s, t), 100 μm (p, q, n′, o′, s′, t′)

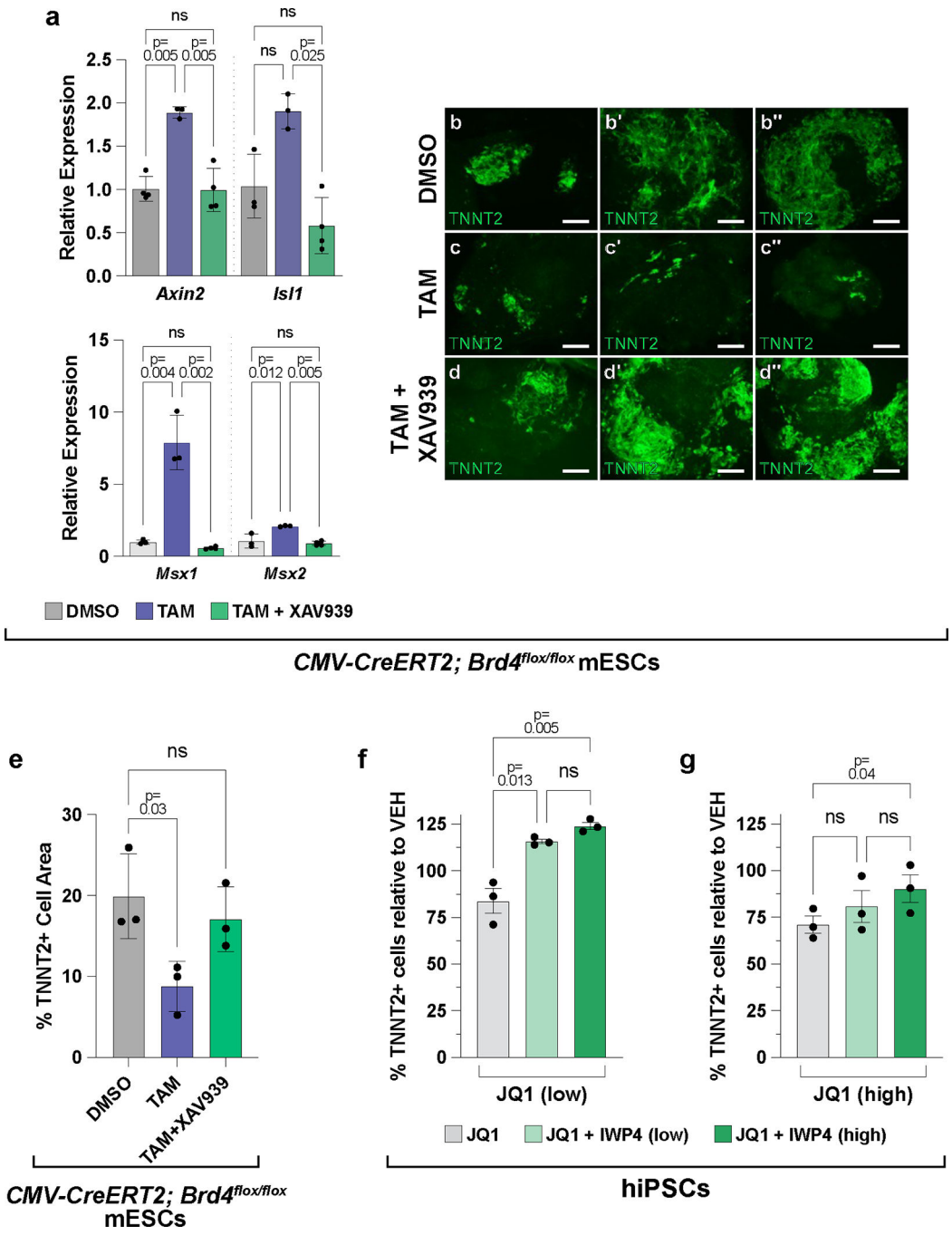

Extended Data Figure 6: BRD4 regulates Wnt signaling during CM differentiation.

(**a**) Attenuating Wnt signaling at the CPC stage (day 5) in mESC to CM differentiation by doubling the normal concentration of the small molecule Wnt inhibitor XAV939 concomitant with *Brd4* genetic deletion by 4-hydroxytamoxifen treatment (TAM) in *CMV-CreERT2; Brd4*$^{flox/flox}$ mESCs partially normalizes expression of CPC markers and *Msx1/2* by qRT-PCR (n=3–4 biologically independent samples per genotype). (**b-e**) Attenuating Wnt signaling at the CPC stage (day 5) in mESC to CM differentiation by doubling the normal concentration of the small molecule Wnt inhibitor XAV939 concomitant with *Brd4*

genetic deletion by 4-hydroxytamoxifen treatment (TAM) in *CMV-CreERT2; Brd4$^{flox/flox}$* mESCs partially normalizes TNNT2 staining by immunofluorescence at day 9 of CM differentiation (for e, n=3 biologically independent samples per condition). (**f,g**) Attenuation of Wnt signaling at the CPC stage (day 6) in hiPSC to CM differentiation by addition of the small molecule Wnt inhibitor IWP4 (5 μM for low dose and 10 μM high dose) concomitant with BET inhibition using JQ1 (25 nM for low dose and 50 nM for high dose) increases the number of TNNT2+ cells as assessed by flow cytometry (n=3 biologically independent samples per condition). Error bars represent ±1 SEM. For a,e,f,g all comparisons are made with p values as indicated (two-way ANOVA with Tukey's multiple comparisons test).

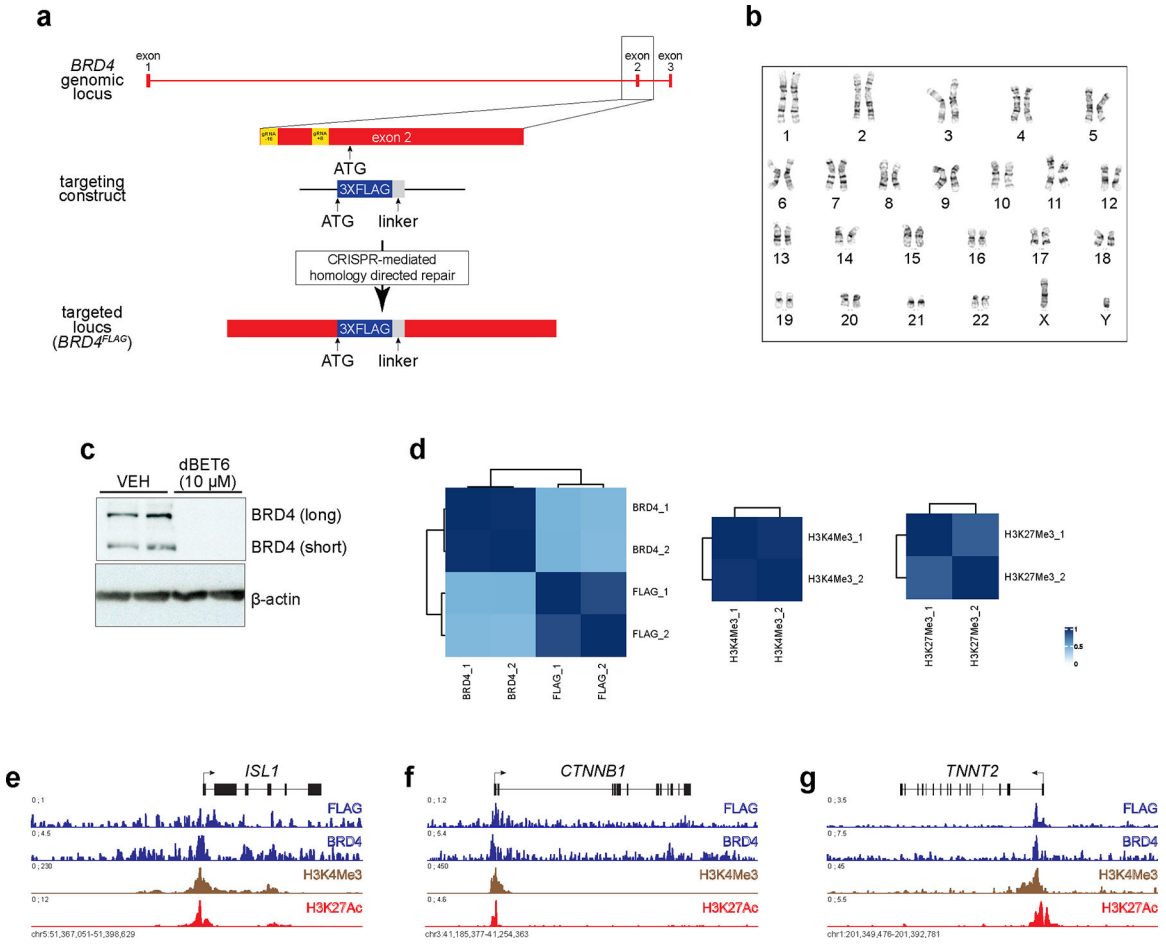

Extended Data Figure 7: Generation of *BRD4$^{FLAG/FLAG}$* hiPSC line and BRD4 occupancy in cardiac progenitor cells.

(**a**) Targeting strategy to introduce 3XFLAG epitope tag into the N-terminus of the endogenous *BRD4* locus. (**b**) Karyotyping results of *BRD4$^{FLAG/FLAG}$* hiPSC line. (**c**) Western blot analysis of protein lysates collected from *BRD4$^{FLAG/FLAG}$* hiPSCs using FLAG antibody demonstrates expression of 3XFLAG-tagged BRD4 isoforms that are degraded upon addition of the PROTAC BET degrader dBET6[51]. (**d**) Pearson correlation matrices demonstrating high reproducibility between replicate CUT&RUN datasets. (**e-g**) Track view of indicated loci showing CUT&RUN factor occupancy (FLAG, BRD4, H3K4Me3) or H3K27Ac ChIP-seq enrichment in hiPSC-derived CPCs.

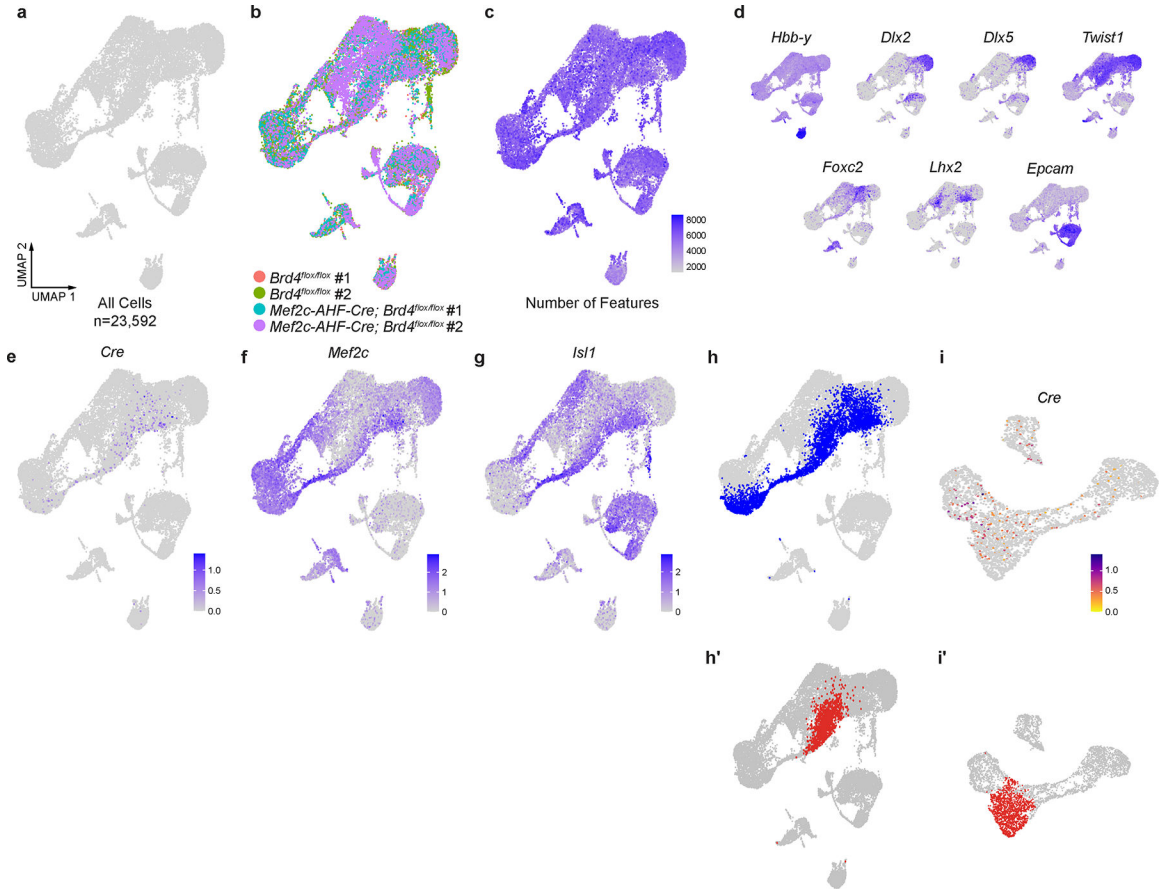

Extended Data Figure 8: Iterative filtering steps for selection of cells analyzed in scRNA-seq.

(**a-c**) UMAP plots of all cells (n=23,592) collected from the microdissected heart and surrounding pharyngeal mesoderm (n=2 embryos per genotype) (a), labeled by sample identity (b), and number of features (c). (**d**) Feature plots for expression of example marker genes used to define cell types (e.g., *Hbb-y* for blood cells; *Dlx2, Dlx5,* and *Twist1* for neural crest cells; *Lhx2* and *Foxc2* for branchiomeric muscle progenitors; *Epcam* for endoderm). (**e-g**) UMAP plots demonstrate expression of the *Cre* transgene (e) occurs in clusters marked by high *Mef2c* (f) and *Isl1* (g) expression, consistent with *Cre* driven in *Mef2c*-expressing second heart field cells. (**h**) Clusters of *Cre* expressing cells detected at E9.5 in our scRNA-seq dataset selected for further analysis (n=4,640). (**i**) Feature plot for *Cre* expression in a UMAP of cells from (h) following normalization and reclustering. (h'-i') Cluster 0 cells highlighted in red on UMAP plots from h and i.

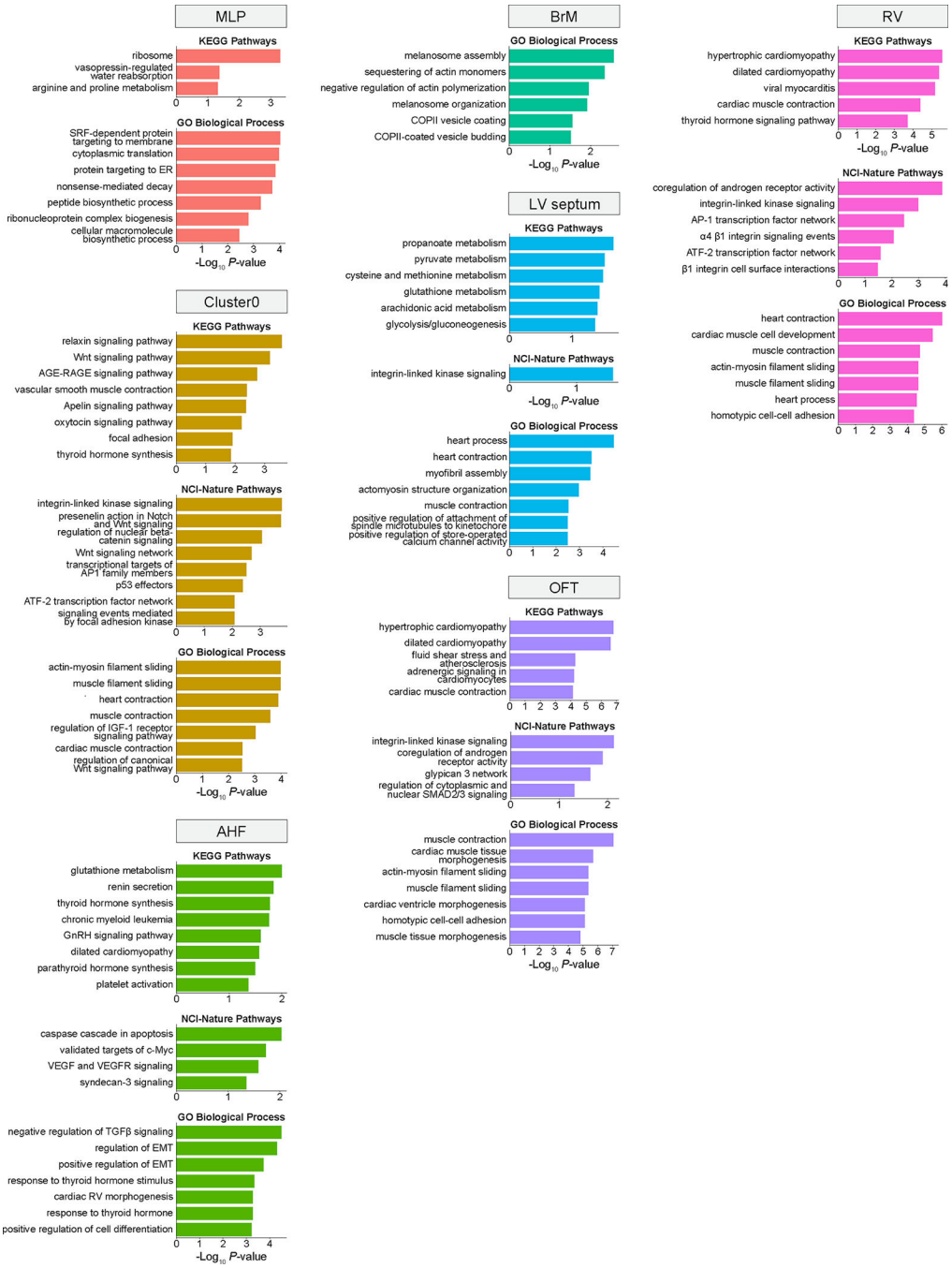

Extended Data Figure 9: Pathway analysis of differentially expressed genes by cluster.
Pathway analysis of differentially expressed genes between mutant (*Mef2c-AHF-Cre; Brd4*$^{flox/flox}$) and control (*Brd4*$^{flox/flox}$) embryos by cluster for each cellular population identified in our scRNA-seq studies (see Methods for details).

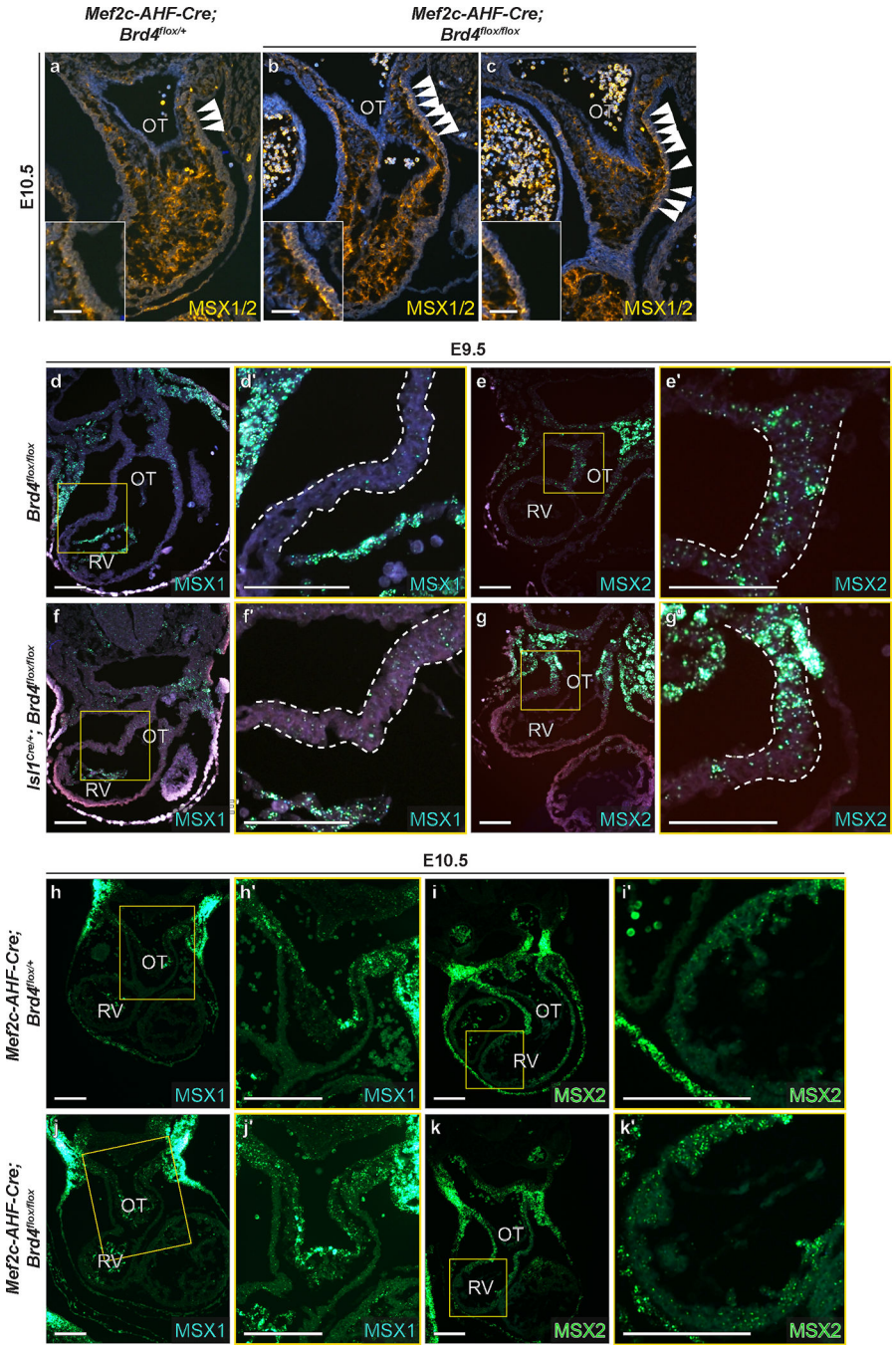

Extended Data Figure 10: BRD4 loss increases MSX1- and MSX2-positive cells *in vivo*.

Mef2c-AHF-Cre; Brd4$^{flox/+}$ (**a**) and *Mef2c-AHF-Cre*; *Brd4*$^{flox/flox}$ (**b,c**) E10.5 embryos at level of right ventricle stained with MSX1/2 (yellow); inset shows area indicated by arrowheads. RNAscope in *Brd4*$^{flox/flox}$ (**d,e**), *Isl1*$^{Cre/+}$; *Brd4*$^{flox/flox}$ (**f,g**), *Mef2c-AHF-Cre*; *Brd4*$^{flox/+}$ (**h,i**), and *Mef2c-AHF-Cre*; *Brd4*$^{flox/flox}$ (**j,k**) E9.5–10.5 embryos at level of right ventricle for MSX1 (d,f,h,j) or MSX2 (e,g,i,k). Regions in yellow boxes in d-k are shown in higher magnification in d′-k′. RV, right ventricle; OT, outflow tract. Scale Bars = 50 μm (a-c, d-k), 165 μm (d′, e′, f′, g′), 125 μm (h′, j′), 200 μm (i′, k′)

Supplementary Material

Refer to Web version on PubMed Central for supplementary material.

Acknowledgments

The authors thank the Srivastava and Jain laboratories for critical discussions and feedback and K. Ozato (National Institutes of Health) for experimental reagents. We are grateful to V. Vedantham (University of California, San Francisco (UCSF)), S. Hota (Gladstone Institutes), I. Kathiriya (UCSF) and M. Costa (Gladstone Institutes) for thoughtful commentary on the manuscript. We thank B. Taylor (Gladstone Institutes) and K. Claiborn (Gladstone Institutes) for editorial assistance as well as A. Silva (Ana Silva Illustrations) and G. Maki (Gladstone Institutes) for assistance with illustrations. We thank the University of Pennsylvania iPSC core for technical assistance. This work was supported by the NIH (R35 HL166663 and R01 HL139783; F31 HL147416 to R.L-S.; K08HL157700 to A.P.; P01 HL146366, R01 HL057181, R01 HL127240 and R01 HL015100 to D.S.), the Burroughs Wellcome Foundation Career Award for Medical Scientists (R.J.), the Allen Foundation (R.J.), the American Heart Association (R.J. and S.M.), the National Science Foundation (15–48571 to R.J.), the Swiss National Science Foundation (P400PM_186704 and P2LAP3_178056 to M.A.), the Japan Society for the Promotion of Science Overseas Research Fellowship (T.N.), the Sarnoff Cardiovascular Research Foundation (A.P.), the Michael Antonov Charitable Foundation (A.P.), the Frank A. Campini Foundation (A.P.), the Tobacco-Related Disease Research Program (578649 to A.P.), the A. P. Giannini Foundation (P0527061 to A.P.), the Roddenberry Foundation (D.S.), the L. K. Whittier Foundation (D.S.), Dario and Irina Sattui (D.S.) and the Younger Family Fund (D.S.).

Data Availability

All data supporting the findings of this study are included in the main article and associated files, and Source Data have been provided with this manuscript. All transcriptomic and epigenomic data are available in the Gene Expression Omnibus database under accession number GSE184922, which is available at https://www.ncbi.nlm.nih.gov/geo/query/acc.cgi?acc=GSE184922.

References

1. Van Der Linde D, Konings EEM & Slager M. a., Witsenburg M, Helbing W. a., Takkenberg JJM & Roos-Hesselink JW Birth prevalence of congenital heart disease worldwide: A systematic review and meta-analysis. J. Am. Coll. Cardiol. 58, 2241–2247 (2011). [PubMed: 22078432]
2. Jin SC et al. Contribution of rare inherited and de novo variants in 2,871 congenital heart disease probands. Nat. Genet. 49, 1593–1601 (2017). [PubMed: 28991257]
3. Pierpont ME et al. Genetic Basis for Congenital Heart Disease: Revisited: A Scientific Statement From the American Heart Association. Circulation 138, e653–e711 (2018). [PubMed: 30571578]
4. de Soysa TY et al. Single-cell analysis of cardiogenesis reveals basis for organ-level developmental defects. Nature 572, 120–124 (2019). [PubMed: 31341279]
5. Homsy J et al. De novo mutations in congenital heart disease with neurodevelopmental and other congenital anomalies. Science 350, 1262–1266 (2015). [PubMed: 26785492]
6. Olley G et al. BRD4 interacts with NIPBL and BRD4 is mutated in a Cornelia de Lange–like syndrome. Nat. Genet. 50, 329–332 (2018). [PubMed: 29379197]
7. Doench JG et al. Optimized sgRNA design to maximize activity and minimize off-target effects of CRISPR-Cas9. Nat. Biotechnol. 34, 184–191 (2016). [PubMed: 26780180]
8. Sapp V et al. Genome-wide CRISPR/Cas9 screening in human iPS derived cardiomyocytes uncovers novel mediators of doxorubicin cardiotoxicity. Sci. Rep. 11, 13866 (2021). [PubMed: 34230586]
9. Chen Y et al. Caveolin-1 Plays an Important Role in the Differentiation of Bone Marrow-Derived Mesenchymal Stem Cells into Cardiomyocytes. Cardiology 136, 40–48 (2017). [PubMed: 27554796]
10. Guo X et al. Cardiomyocyte differentiation of mesenchymal stem cells from bone marrow: new regulators and its implications. Stem Cell Res. Ther. 9, 44 (2018). [PubMed: 29482607]

11. Singh AM et al. Chibby, an antagonist of the Wnt/beta-catenin pathway, facilitates cardiomyocyte differentiation of murine embryonic stem cells. Circulation 115, 617–626 (2007). [PubMed: 17261658]
12. Kim M-S et al. Activin-A and Bmp4 levels modulate cell type specification during CHIR-induced cardiomyogenesis. PLoS One 10, e0118670 (2015). [PubMed: 25706534]
13. Morton SU, Quiat D, Seidman JG & Seidman CE Genomic frontiers in congenital heart disease. Nat. Rev. Cardiol. (2021) doi:10.1038/s41569-021-00587-4.
14. Dong C et al. Comparison and integration of deleteriousness prediction methods for nonsynonymous SNVs in whole exome sequencing studies. Hum. Mol. Genet. 24, 2125–2137 (2015). [PubMed: 25552646]
15. Krumm N et al. Excess of rare, inherited truncating mutations in autism. Nat. Genet. 47, 582–588 (2015). [PubMed: 25961944]
16. Struhl K Histone acetylation and transcriptional regulatory mechanisms. Genes Dev. 12, 599–606 (1998). [PubMed: 9499396]
17. Szklarczyk D et al. STRING v11: protein-protein association networks with increased coverage, supporting functional discovery in genome-wide experimental datasets. Nucleic Acids Res. 47, D607–D613 (2019). [PubMed: 30476243]
18. Han P, Hang CT, Yang J & Chang C-P Chromatin remodeling in cardiovascular development and physiology. Circ. Res. 108, 378–396 (2011). [PubMed: 21293009]
19. Padmanabhan A & Haldar SM Drugging transcription in heart failure. J. Physiol. 598, 3005–3014 (2020). [PubMed: 30927446]
20. Lovén J et al. Selective Inhibition of Tumor Oncogenes by Disruption of Super-Enhancers. Cell vol. 153 320–334 Preprint at 10.1016/j.cell.2013.03.036 (2013). [PubMed: 23582323]
21. Filippakopoulos P et al. Selective inhibition of BET bromodomains. Nature 468, 1067–1073 (2010). [PubMed: 20871596]
22. Lee J-E et al. Brd4 binds to active enhancers to control cell identity gene induction in adipogenesis and myogenesis. Nat. Commun. 8, 1–12 (2017). [PubMed: 28232747]
23. Zengerle M, Chan K-H & Ciulli A Selective Small Molecule Induced Degradation of the BET Bromodomain Protein BRD4. ACS Chem. Biol. 10, 1770–1777 (2015). [PubMed: 26035625]
24. Yang L et al. Isl1Cre reveals a common Bmp pathway in heart and limb development. Development 133, 1575–1585 (2006). [PubMed: 16556916]
25. Padmanabhan A et al. BRD4 (Bromodomain-Containing Protein 4) Interacts with GATA4 (GATA Binding Protein 4) to Govern Mitochondrial Homeostasis in Adult Cardiomyocytes. Circulation 142, 2338–2355 (2020). [PubMed: 33094644]
26. Linares-Saldana R et al. BRD4 orchestrates genome folding to promote neural crest differentiation. Nat. Genet. 53, 1480–1492 (2021). [PubMed: 34611363]
27. Jain R et al. HEART DEVELOPMENT. Integration of Bmp and Wnt signaling by Hopx specifies commitment of cardiomyoblasts. Science 348, aaa6071 (2015). [PubMed: 26113728]
28. Cai C-L et al. Isl1 identifies a cardiac progenitor population that proliferates prior to differentiation and contributes a majority of cells to the heart. Dev. Cell 5, 877–889 (2003). [PubMed: 14667410]
29. Verzi MP, McCulley DJ, De Val S, Dodou E & Black BL The right ventricle, outflow tract, and ventricular septum comprise a restricted expression domain within the secondary/anterior heart field. Dev. Biol. 287, 134–145 (2005). [PubMed: 16188249]
30. Kwon C et al. Canonical Wnt signaling is a positive regulator of mammalian cardiac progenitors. Proc. Natl. Acad. Sci. U. S. A. 104, 10894–10899 (2007). [PubMed: 17576928]
31. Gessert S & Kühl M The multiple phases and faces of wnt signaling during cardiac differentiation and development. Circ. Res. 107, 186–199 (2010). [PubMed: 20651295]
32. Cohen ED et al. Wnt/beta-catenin signaling promotes expansion of Isl-1-positive cardiac progenitor cells through regulation of FGF signaling. J. Clin. Invest. 117, 1794–1804 (2007). [PubMed: 17607356]
33. Jho E-H et al. Wnt/beta-catenin/Tcf signaling induces the transcription of Axin2, a negative regulator of the signaling pathway. Mol. Cell. Biol. 22, 1172–1183 (2002). [PubMed: 11809808]

34. Zhao M-T et al. Cell Type-Specific Chromatin Signatures Underline Regulatory DNA Elements in Human Induced Pluripotent Stem Cells and Somatic Cells. Circ. Res. 121, 1237–1250 (2017). [PubMed: 29030344]
35. Devine WP, Wythe JD, George M, Koshiba-Takeuchi K & Bruneau BG Early patterning and specification of cardiac progenitors in gastrulating mesoderm. Elife 3, (2014).
36. Lescroart F et al. Defining the earliest step of cardiovascular lineage segregation by single-cell RNA-seq. Science 359, 1177–1181 (2018). [PubMed: 29371425]
37. Nomaru H et al. Single cell multi-omic analysis identifies a Tbx1-dependent multilineage primed population in the murine cardiopharyngeal mesoderm. bioRxiv 2020.12.24.424342 (2020) doi:10.1101/2020.12.24.424342.
38. Chen Y-H, Ishii M, Sun J, Sucov HM & Maxson RE Jr. Msx1 and Msx2 regulate survival of secondary heart field precursors and post-migratory proliferation of cardiac neural crest in the outflow tract. Dev. Biol. 308, 421–437 (2007). [PubMed: 17601530]
39. Song L et al. Lrp6-mediated canonical Wnt signaling is required for lip formation and fusion. Development 136, 3161–3171 (2009). [PubMed: 19700620]
40. Rao J et al. Stepwise Clearance of Repressive Roadblocks Drives Cardiac Induction in Human ESCs. Cell Stem Cell 18, 341–353 (2016). [PubMed: 26748419]
41. Gonzalez-Teran B et al. Transcription factor protein interactomes reveal genetic determinants in heart disease. Cell 185, 794–814.e30 (2022). [PubMed: 35182466]
42. Dawson MA The cancer epigenome: Concepts, challenges, and therapeutic opportunities. Science 355, 1147–1152 (2017). [PubMed: 28302822]
43. Dey A et al. BRD4 directs hematopoietic stem cell development and modulates macrophage inflammatory responses. EMBO J. 38, e100293 (2019). [PubMed: 30842097]
44. Chatfield KC et al. Congenital heart disease in Cornelia de Lange syndrome: phenotype and genotype analysis. Am. J. Med. Genet. A 158A, 2499–2505 (2012). [PubMed: 22965847]
45. Li F-F et al. Characterization of Transcriptional Repressor Gene MSX1 Variations for Possible Associations with Congenital Heart Diseases. PLoS One 10, e0142666 (2015). [PubMed: 26556783]
46. Lahm H et al. Congenital heart disease risk loci identified by genome-wide association study in European patients. J. Clin. Invest. 131, (2021).
47. Ivanovitch K et al. Ventricular, atrial, and outflow tract heart progenitors arise from spatially and molecularly distinct regions of the primitive streak. PLoS Biol. 19, e3001200 (2021). [PubMed: 33999917]
48. Boogerd CJJ, Moorman AFM & Barnett P Expression of muscle segment homeobox genes in the developing myocardium. Anat. Rec. 293, 998–1001 (2010).
49. Qi LS et al. Repurposing CRISPR as an RNA-guided platform for sequence-specific control of gene expression. Cell 152, 1173–1183 (2013). [PubMed: 23452860]
50. Muzumdar MD, Tasic B, Miyamichi K, Li L & Luo L A global double-fluorescent Cre reporter mouse. Genesis 45, 593–605 (2007). [PubMed: 17868096]
51. Yang W et al. Generation of iPSCs as a Pooled Culture Using Magnetic Activated Cell Sorting of Newly Reprogrammed Cells. PLoS One 10, e0134995 (2015). [PubMed: 26281015]
52. Kreitzer FR et al. A robust method to derive functional neural crest cells from human pluripotent stem cells. Am. J. Stem Cells 2, 119–131 (2013). [PubMed: 23862100]
53. Manipulating the Mouse Embryo: A Laboratory Manual 3rd Edn. (Cold Spring Harbor Laboratory Press, 2003).
54. Poleshko A et al. Genome-Nuclear Lamina Interactions Regulate Cardiac Stem Cell Lineage Restriction. Cell 171, 573–587.e14 (2017). [PubMed: 29033129]
55. Christoforou N et al. Mouse ES cell–derived cardiac precursor cells are multipotent and facilitate identification of novel cardiac genes. J. Clin. Invest. 118, 894–903 (2008). [PubMed: 18246200]
56. Kattman SJ et al. Stage-Specific Optimization of Activin/Nodal and BMP Signaling Promotes Cardiac Differentiation of Mouse and Human Pluripotent Stem Cell Lines. Cell Stem Cell vol. 8 228–240 Preprint at 10.1016/j.stem.2010.12.008 (2011). [PubMed: 21295278]

57. Shah PP et al. Pathogenic LMNA variants disrupt cardiac lamina-chromatin interactions and de-repress alternative fate genes. Cell Stem Cell 28, 938–954.e9 (2021). [PubMed: 33529599]
58. Lian X et al. Robust cardiomyocyte differentiation from human pluripotent stem cells via temporal modulation of canonical Wnt signaling. Proc. Natl. Acad. Sci. U. S. A. 109, E1848–57 (2012). [PubMed: 22645348]
59. Luo B et al. Highly parallel identification of essential genes in cancer cells. Proc. Natl. Acad. Sci. U. S. A. 105, 20380–20385 (2008). [PubMed: 19091943]
60. Dobin A et al. STAR: ultrafast universal RNA-seq aligner. Bioinformatics 29, 15–21 (2013). [PubMed: 23104886]
61. Liao Y, Wang J, Jaehnig EJ, Shi Z & Zhang B WebGestalt 2019: gene set analysis toolkit with revamped UIs and APIs. Nucleic Acids Res. 47, W199–W205 (2019). [PubMed: 31114916]
62. Robinson MD, McCarthy DJ & Smyth GK edgeR: a Bioconductor package for differential expression analysis of digital gene expression data. Bioinformatics vol. 26 139–140 Preprint at 10.1093/bioinformatics/btp616 (2010). [PubMed: 19910308]
63. Robinson M, McCarthy DJ, Chen Y & Smyth GK Package ‘edger’. Preprint at http://citeseerx.ist.psu.edu/viewdoc/download?doi=10.1.1.367.3149&rep=rep1&type=pdf (2012).
64. Stuart T et al. Comprehensive Integration of Single-Cell Data. Cell 177, 1888–1902.e21 (2019). [PubMed: 31178118]
65. Street K et al. Slingshot: cell lineage and pseudotime inference for single-cell transcriptomics. BMC Genomics 19, 477 (2018). [PubMed: 29914354]
66. Cheshire C et al. Nf-Core/cutandrun: Nf-Core/cutandrun v3.2 Tin Albatross. (2023). doi:10.5281/zenodo.8305872.

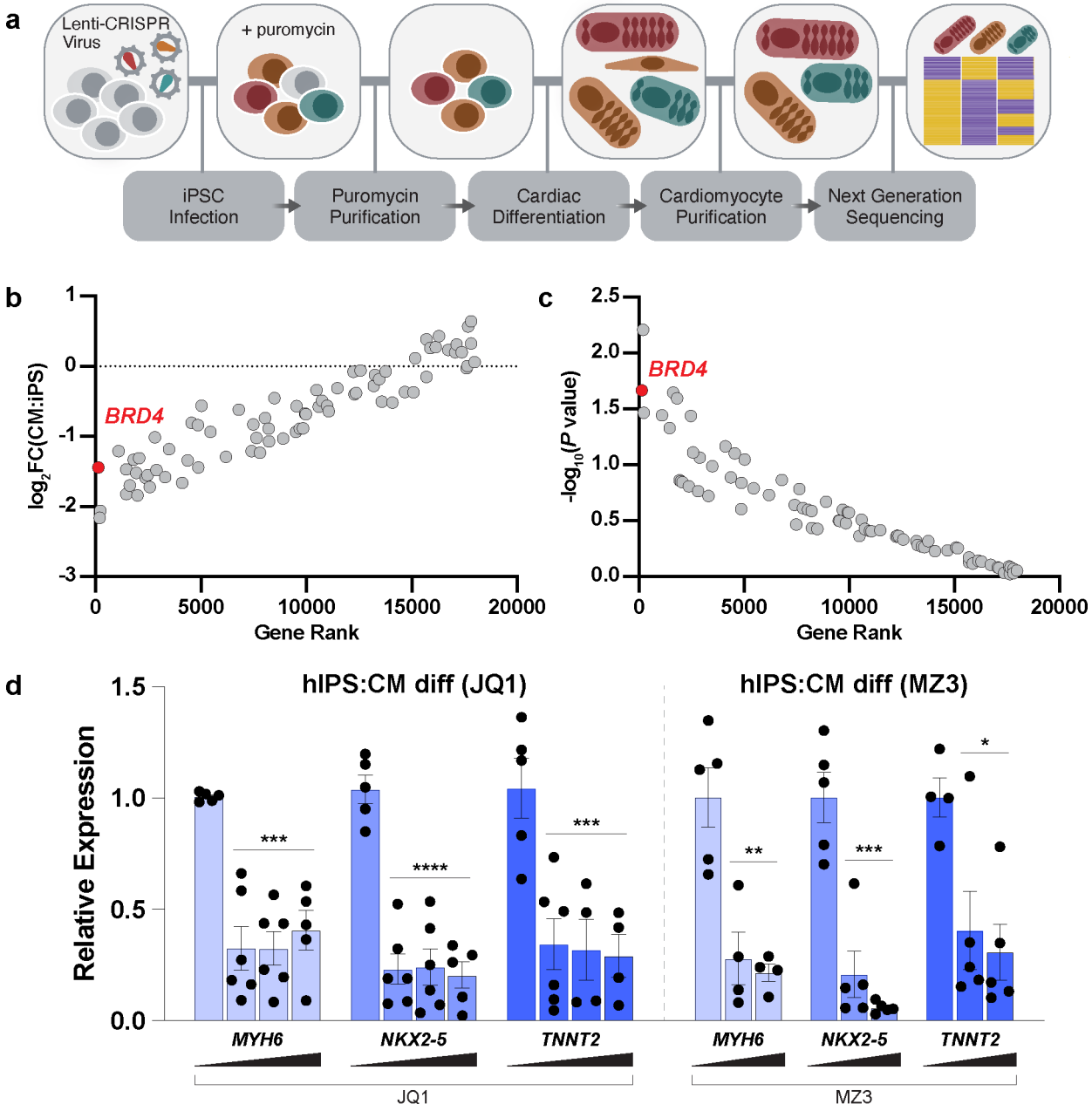

Fig. 1: A pooled CRISPR screen identifies BRD4 as a regulator of cardiogenesis.

a, Schematic representation of screen. **b,** Hits for chromatin-associated proteins ranked by fold enrichment in CMs compared to hiPSCs. **c,** Hits for chromatin-associated proteins ranked by *P* value (see Methods for details). **d,** Expression of *MYH6, NKX2–5* and *TNNT2* at day 12 of cardiac differentiation (JQ1 or MZ3 added at day 6 corresponding to the CPC stage; JQ1 concentrations: 0, 25, 100, 250 nM; MZ3: 0, 200, 500 nM (n = 4–6 biologically independent samples)). In all graphs, error bars represent ±1 SEM. For d, all comparisons are made relative to 0 nM compound for each gene; **P* < 0.0248, ***P* < 0.0048, ****P* < 0.002, *****P* < 0.0001 (two-tailed unpaired t-test).

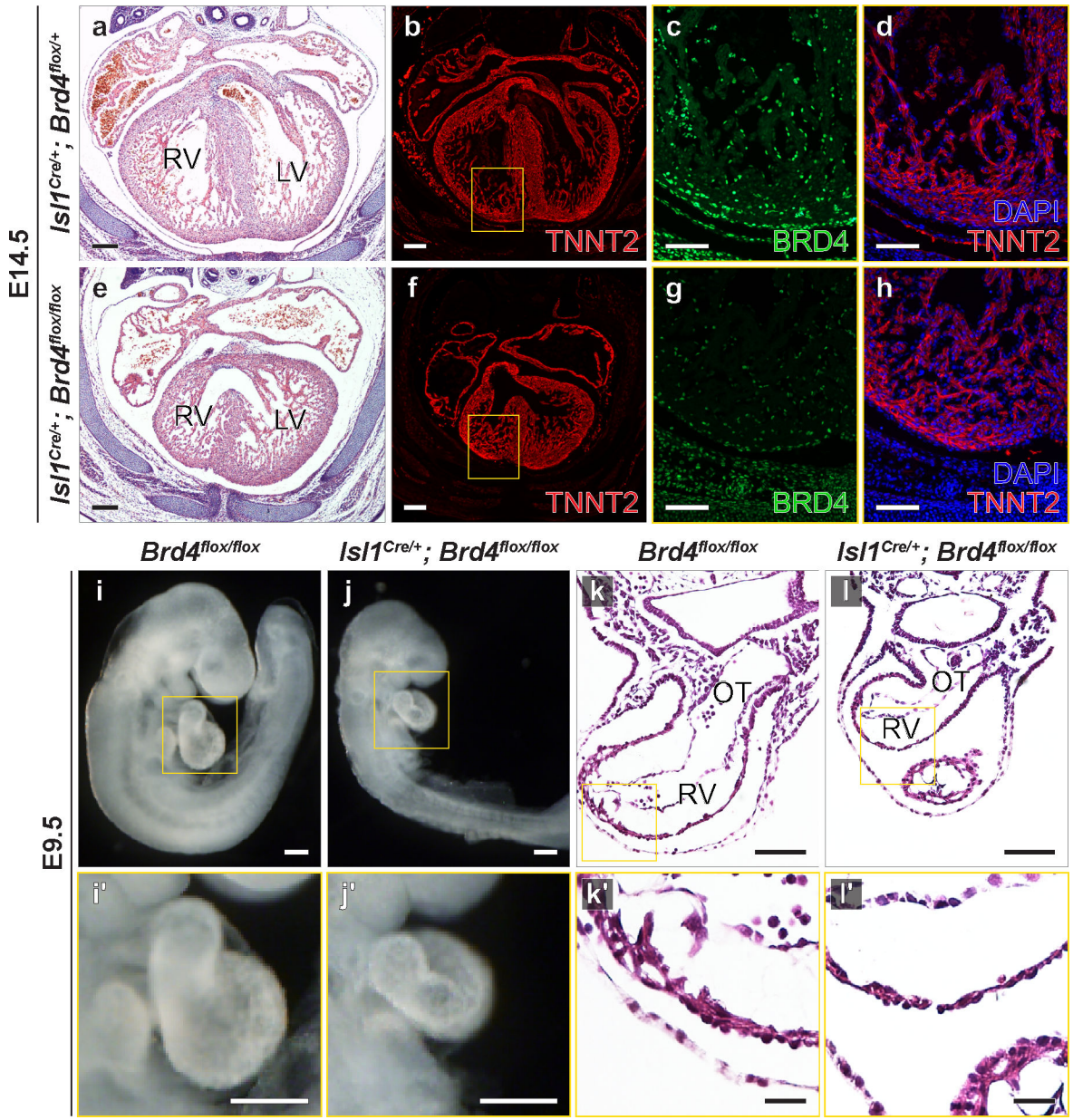

Fig. 2: *Brd4* deletion in ISL1+ progenitors *in vivo* results in myocardial hypoplasia.

a-h, H&E staining (a,e) and immunohistochemistry (b-d, f-h) of *Isl1*$^{Cre/+}$; *Brd4*$^{flox/+}$ (b-d) and *Isl1*$^{Cre/+}$; *Brd4*$^{flox/flox}$ (f-h) E14.5 hearts. Immunohistochemistry of Tnnt2 (red) and BRD4 (green). **i,j,** *Isl1*$^{Cre/+}$; *Brd4*$^{flox/+}$ (i,i′) and *Isl1*$^{Cre/+}$; *Brd4*$^{flox/flox}$ (j,j′) E9.5 embryos. Regions in yellow boxes in i and j are shown in higher magnification in i′ and j′. **k,l,** H&E staining of a section through OFT and RV of *Isl1*$^{Cre/+}$; *Brd4*$^{flox/+}$ (k,k′) and *Isl1*$^{Cre/+}$; *Brd4*$^{flox/flox}$ (l,l′) E9.5 embryos. Regions in yellow boxes in k and l are shown in higher magnification in k′ and l′. Scale bars, 200 μm (a,b,e,f), 100 μm (c,d,g,h,k,l), 250 μm (i,i′,j,j′) and 25 μm (k′,l′),

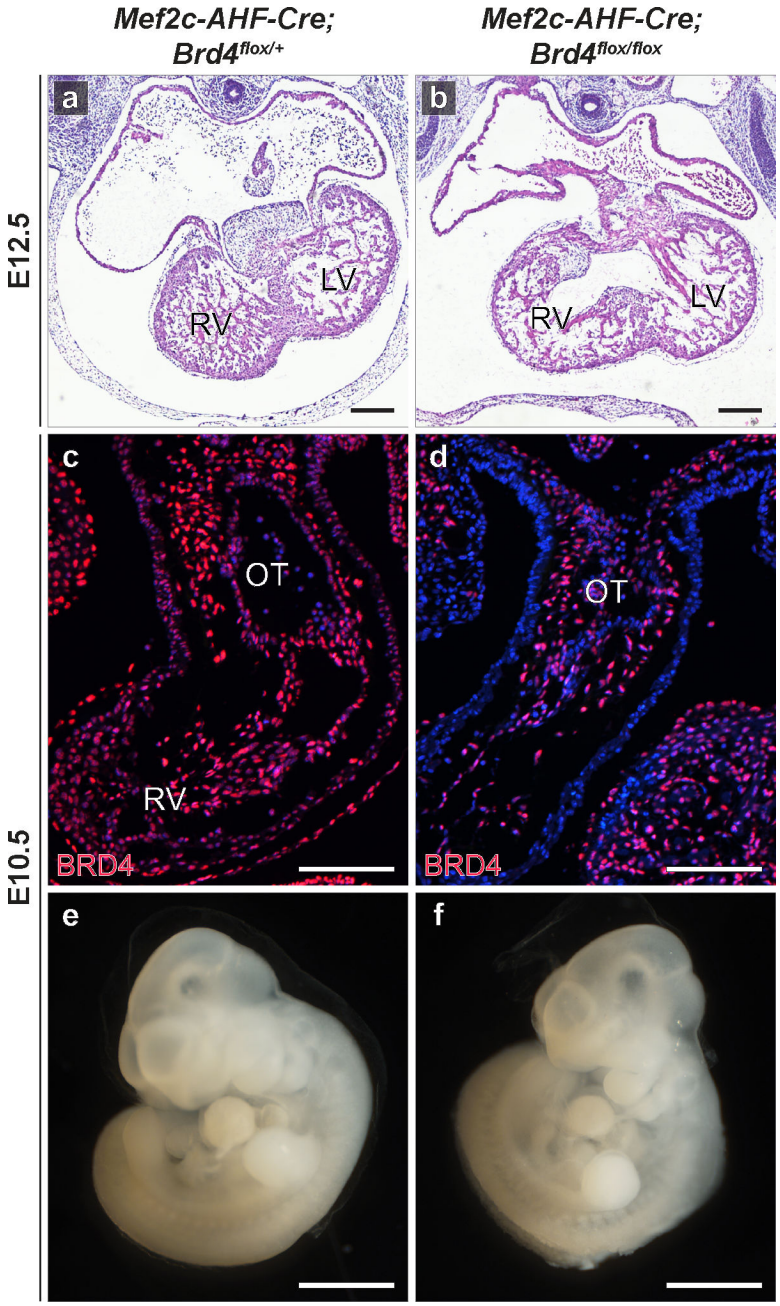

Fig. 3: *Brd4* deletion in SHF progenitors *in vivo* recapitulates loss in ISL1+ progenitors.
a,b, H&E staining of *Mef2c-AHF-Cre*; $Brd4^{flox/+}$ (a) and *Mef2c-AHF-Cre*; $Brd4^{flox/flox}$ (b) E12.5 hearts. Note the RV hypoplasia in the mutant compared to control. **c,d,** Immunohistochemistry of BRD4 in *Mef2c-AHF-Cre*; $Brd4^{flox/+}$ (c) and *Mef2c-AHF-Cre*; $Brd4^{flox/flox}$ (d) E10.5 OFTs. **e,f,** *Mef2c-AHF-Cre*; $Brd4^{flox/+}$ (e) and *Mef2c-AHF-Cre*; $Brd4^{flox/flox}$ (f) E10.5 embryos. Scale bars, 100 μm (a-d) and 250 μm (e,f)

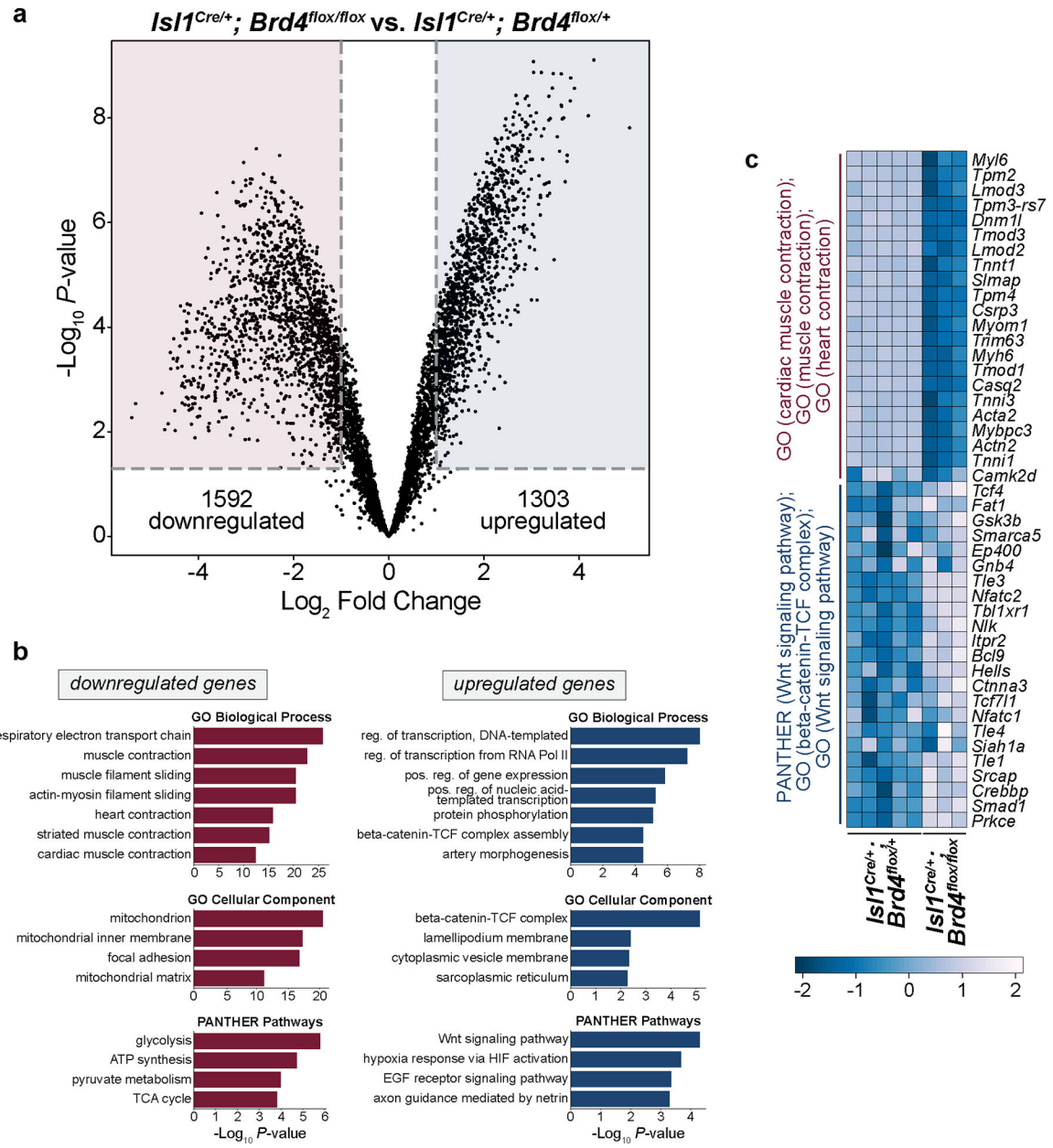

Fig. 4: Loss of BRD4 *in vivo* attenuates cardiac differentiation-related gene expression.

a, Volcano plot of E9.5 *Isl1*$^{Cre/+}$; *Brd4*$^{flox/+}$ versus *Isl1*$^{Cre/+}$; *Brd4*$^{flox/flox}$ embryonic hearts ranked by *P* value (see Methods for details). **b,** GO analysis of top downregulated and upregulated genes (see Methods for details). **c,** Heat map showing expression of CM function and Wnt-related genes at E9.5 (see Methods for details).

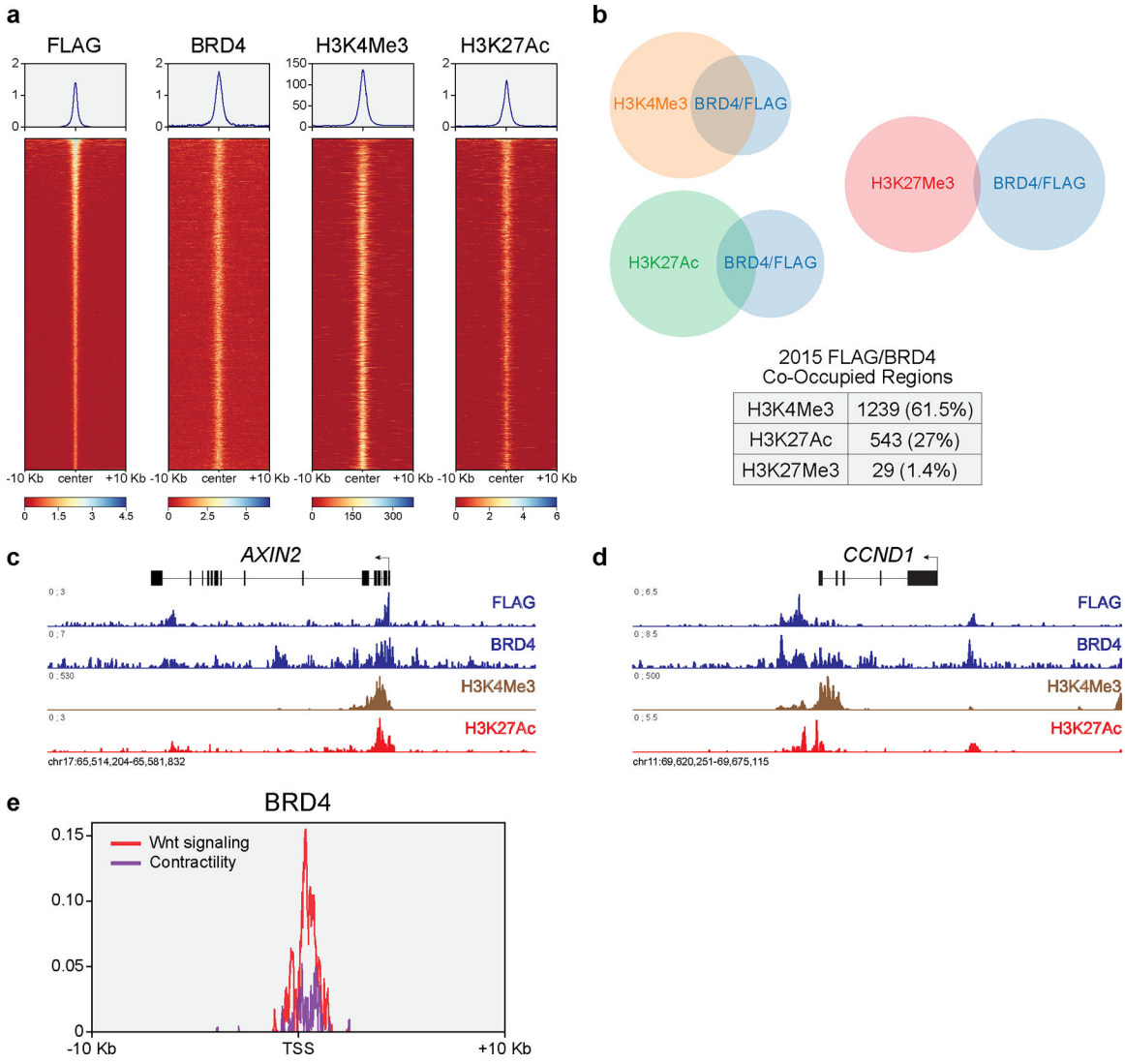

Fig. 5: BRD4 is enriched at transcriptionally active regions of chromatin marked by H3K4Me3.

a, Heat maps showing enrichment of FLAG, BRD4 and H3K4Me3 CUT&RUN signals and H3K27Ac ChIP-seq[34] enrichment from hiPSC-derived CPCs at day 6 ordered by FLAG intensity. **b,** Venn diagrams and table demonstrating co-occupancy of BRD4/FLAG and indicated histone modification (percentage of BRD4 peaks overlapping with indicated histone modification). **c,d,** Track view of *AXIN2* (c) and *CCND1* (d) loci showing indicated CUT&RUN factor occupancy or H3K27Ac ChIP-seq enrichment in hiPSC-derived CPCs. **e,** Metaplot demonstrating FLAG occupancy at genes associated with GO terms for Wnt signaling or contractility. ChIP-seq, chromatin immunoprecipitation followed by sequencing.

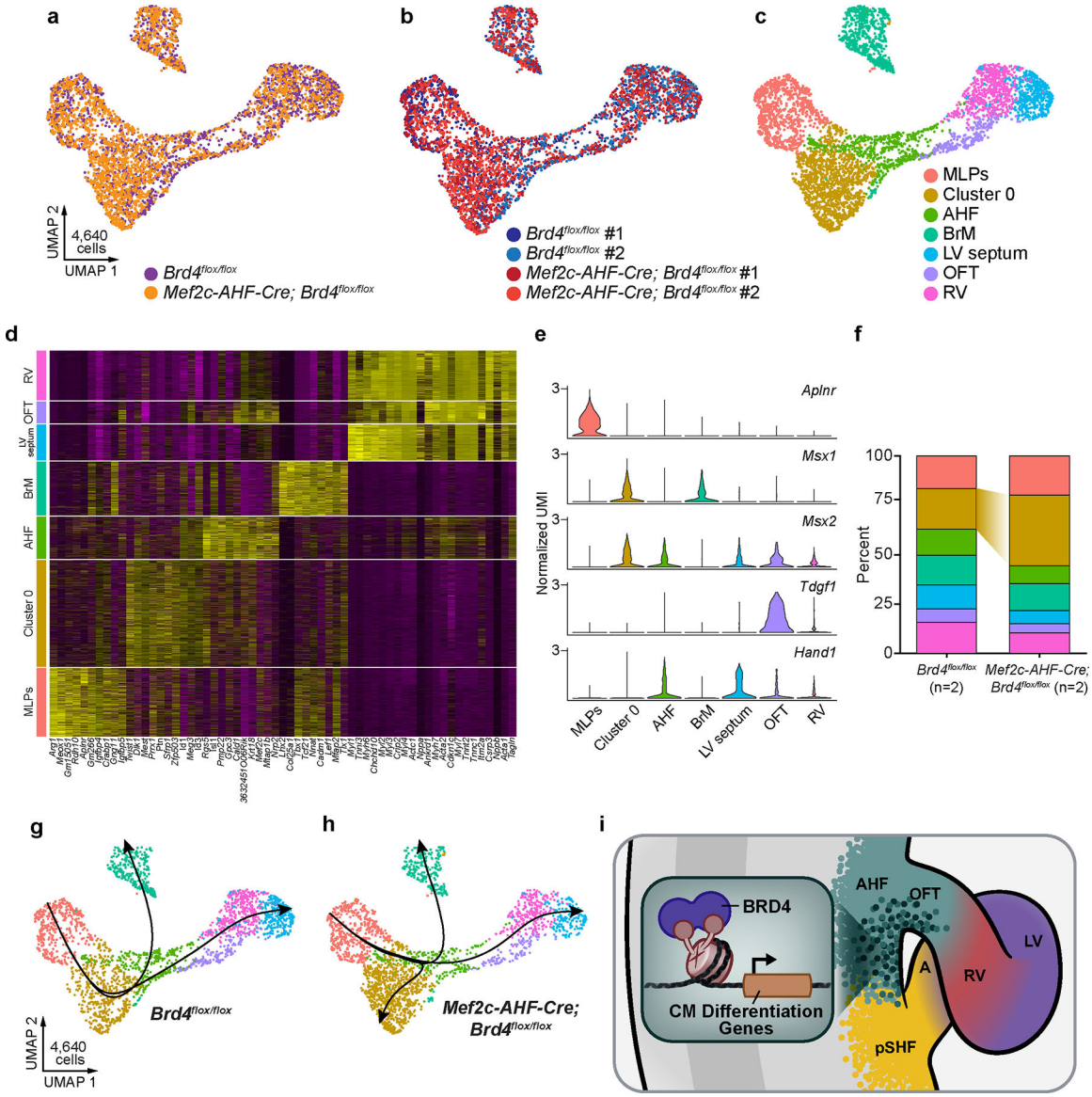

Fig. 6: BRD4 specifically regulates an MSX1/2+ progenitor population.

a-c, UMAP plots of single-cell gene expression of *Brd4*$^{flox/flox}$ (n = 2) and *Mef2c-AHF-Cre*; *Brd4*$^{flox/flox}$ (n = 2) embryos visualized by genotype (a), sample identity (b), or cluster identity (c). **d,** Gene expression analysis of single-cell data. Heat map shows genes most enriched in each cluster and their inferred identity. **e,** Violin plots showing gene expression of critical regulators in select clusters. **f,** Percentage of cells in each cluster in each genotype highlighting the expansion of cluster 0 (MSX1/2+ progenitors) upon BRD4 deletion. **g,h,** Multiple lineage and pseudotime trajectory inference of cells from control (*Brd4*$^{flox/flox}$) (g) and mutant (*Mef2c-AHF-Cre; Brd4*$^{flox/flox}$) (h) embryos. **i,** Proposed model for BRD4 action in SHF CPCs: BRD4 is critical for CM differentiation in a subset of SHF CPCs, with its loss leading to persistence of Wnt-activated, ISL1+, and MSX1/2+ CPCs. A, atrium; pSHF, posterior second heart field.